frontiers in Earth Science

ORIGINAL RESEARCH
published: 11 March 2022
doi: 10.3389/feart.2022.830453

# Discovery of Yaozhuang Stock and Deep Ore Prospecting Implication for the Western Mangling Orefield in North Qinling Terrane, Central China

*Peng Fan*[1,2], *Aihua Xi*[1]*, *Bin Zhou*[2], *Xu Chao*[2], *Wenbo Yang*[2], *Jiaxin Sun*[2], *Hongyu Zhu*[2] and *Li Wei*[2]

[1]State Key Laboratory of Oil and Gas Reservoir Geology and Exploitation, Southwest Petroleum University, Chengdu, China, [2]Shaanxi Geological Survey Planning Research Center (Shaanxi Geological Survey Fund Center), Xi'an, China

In the western Mangling orefield, the molybdenum (Mo) polymetallic deposits are closely related to the ore-bearing porphyry stocks (individual outcrop size: <1 $km^2$). In this study, we have discovered several granitic stocks at Yaozhuang. Systematic petrologic, zircon U-Pb-Hf isotope and whole-rock geochemical studies show that both the granitic stocks of porphyritic granite (157 ± 2 Ma) and the intruding monzogranite dike (153 ± 1 Ma) were emplaced in the Late Jurassic. These granitic stocks are characterized by high $SiO_2$ (66.83–75.63 wt%), high $K_2O$ (4.15–5.05 wt%), high $Al_2O_3$ (12.90–16.93 wt%), and low MgO (0.06–0.73 wt%) and are metaluminous to weakly peraluminous, being highly fractionated I-A-type transition granites. The content of the total rare Earth element (ΣREE) of the porphyritic granite (139.6–161.7 ppm) is lower than that of the monzogranite (151.4–253.6 ppm). The porphyritic granite has weakly negative Eu anomalies (Eu/Eu* = 0.77–0.93), whereas the monzogranite has weakly positive Eu anomalies (Eu/Eu* = 0.97–1.21) and are more enriched in light rare Earth elements. Both of them are enriched in large ion lithophile elements (LILEs, e.g., K, Rb, and Ba) but depleted in high-field-strength elements (HFSEs, e.g., Nb, Ta, Ti, Zr, and Hf). The zircon $\varepsilon_{Hf}(t)$ values of all the samples range from −16.1 to −6.9, and the two-stage model ages ($t_{DM2}$) are 1.78–2.16 Ga. The magma may have originated from partial melting of the lower crust (more than 40 km in depth) caused by mantle-derived magma underwelling. The plutons and stocks were emplaced into the intersection of the early EW-trending faults and the late (Yanshanian) NE-trending faults. The fertile magma with high water content ($H_2O$ > 4%) and high oxygen fugacity (Delta FMQ > 1.5) indicates that the Yaozhuang area has significant potential for porphyry Mo polymetallic ore discovery.

**Keywords: Yaozhuang granitic stocks, zircon U-Pb age, late Jurassic granite, western Mangling orefield, North Qinling terrane**

OPEN ACCESS

***Edited by:***
*Kit Lai,*
*Universiti Brunei Darussalam, Brunei*

***Reviewed by:***
*Rui Wang,*
*China University of Geosciences, China*
*Jian-Jun Fan,*
*Jilin University, China*

***Correspondence:**
*Aihua Xi*
*aihuaxi@163.com*

***Specialty section:***
*This article was submitted to Geochemistry, a section of the journal Frontiers in Earth Science*

***Received:*** *07 December 2021*
***Accepted:*** *17 January 2022*
***Published:*** *11 March 2022*

***Citation:***
*Fan P, Xi A, Zhou B, Chao X, Yang W, Sun J, Zhu H and Wei L (2022) Discovery of Yaozhuang Stock and Deep Ore Prospecting Implication for the Western Mangling Orefield in North Qinling Terrane, Central China. Front. Earth Sci. 10:830453. doi: 10.3389/feart.2022.830453*

**Abbreviations:** A, A-type granite; FG, differentiated granite; I, S, and M, undifferentiated I, S, and M-type granite; OGT, undifferentiated I, S, and M-type granite.

## INTRODUCTION

The Qinling orogen is well-known for its multistage magmatism and orogeny (Mattauer et al., 1985; Kröner et al., 1998; Meng and Zhang, 1999; Liu et al., 2016). The magmatism occurred in four major stages: Neoproterozoic, Paleozoic, Early Mesozoic, and Late Mesozoic (Ratschbacher et al., 2003; Wang et al., 2012; Wang et al., 2015b). Previous works have studied the rock assemblage, magma source, and spatiotemporal evolution of intermediate-felsic plutons in the region and described the multistage orogeny in detail (Zhang et al., 1995; Dong et al., 2012; 2016; Wang et al., 2017; Li N. et al., 2018; Bao et al., 2019).

The western Mangling orefield is one of the deep prospecting hotspots in North Qinling terrane in recent years, and the orefield is also an important component of the Qinling Mo polymetallic ore belt (Fan and Xie, 1999; Mao et al., 2011; Yang et al., 2017). The known deposits in the area include Taoguanping, Xigou, Nantai, Mahe Mo deposits, etc. The Late Jurassic–Early Cretaceous Mangling pluton and the western porphyries are developed in the orefield, and the latter is closely related to the local Mo polymetallic mineralization (Mao et al., 2008, 2010; Zeng et al., 2012; Zhai and Santosh, 2013). In recent years, many workers have studied the age, magma evolution, petrogenesis, and mineralization of the Mangling pluton and Nantai, Taoguanping, and Xigou granitic stocks on the western side of the orefield (Ke et al., 2012a, 2012b; Qin et al., 2012; Yang et al., 2014; Hu et al., 2017), whereas granitic stock in the Yaozhuang area was rarely studied. The 1:50,000 gravity survey in Mangling revealed an oval low Bouguer gravity anomaly at Yaozhuang, and the presence of concealed porphyry bodies was speculated at depth (Yang et al., 2020). In the southwest of the study area, the borehole (Northwest Nonferrous Geological Research Institute Co., Ltd.) drilled porphyry at 380–1,400 m, accompanied by NW-extending Mo polymetallic ore (Yang et al., 2019). In the process of field geological survey, Yaozhuang stock and some monzogranite dikes were found near the gravity anomaly. Therefore, we analyzed the zircon U-Pb geochronology, Lu-Hf isotopes, and whole-rock geochemistry of the Yaozhuang stocks and discussed their petrogenesis and prospecting implications for the western Mangling orefield. This work provides new data for studying the late Mesozoic tectonic–magmatic evolution of the North Qinling terrane.

## GEOLOGICAL SETTING

The study area (Yaozhuang, Luonan County) in North Qinling is located in the early Neoproterozoic Kuanping Rift, a narrow EW-trending structure extending along the Luonan–Luanchuan and Qiaorui–Waxuezi deep-seated faults (Zhang S. H. et al., 2019). Among them, there are a large number of NE-trending Yanshanian faults. The intersection of these faults often controls the development of various magmatic deposits (Diwu et al., 2010). Exposed stratigraphy comprises predominantly the Middle-Upper Proterozoic Kuanping Group ($Pt_{2-3}k$), consisting of metamorphosed mafic volcanic rocks, clastic rocks, and carbonate rocks. The Kuanping Group can be divided into the Guangdongping ($Pt_{2-3}gd$), Sichakou ($Pt_{2-3}sc$), and Xiewan ($Pt_{2-3}x$) formations from bottom to top (Li C. D. et al., 2018). The crystalline basement comprises the Qinling Group amphibolite-facies metamorphic rocks, with local granulite- or eclogite-facies rocks (Liu B. X. et al., 2013; Diwu et al., 2014; Zhang et al., 2015). There are a series of Yanshanian (Jurassic–Cretaceous) granitic stocks in the area. The Mangling pluton is a large EW-trending intrusive complex, containing diorite, biotite monzogranite, and moyite. On the western side of the Mangling pluton, shallow granitic stocks (e.g., Taoguanping, Xigou, Nantai, and Panhe) are present with lithology mainly of porphyritic granite, monzogranite, alaskite, and granodiorite (**Figure 1**).

The Yaozhuang granitic stocks intruded the Sichakou Formation biotite-quartz schist and the Guangdongping Formation plagioclase-amphibole schist. The individual stock has an exposed area of $<1\ km^2$ and extends NW or NE (**Figure 2A**). These stocks comprise mainly porphyritic granite and intruding monzogranite dikes (**Figure 2B**).

## SAMPLES AND ANALYTICAL METHODS

### Sample Descriptions

Ten samples (five porphyritic granite and five monzogranite) in this study were collected from Yaozhuang village, Luonan County. The sampling positions are shown in **Figure 1**.

The porphyritic granite is light gray and massive and composed of phenocrysts (15 vol%) and groundmass (85 vol %). The phenocrysts comprise mainly plagioclase, K-feldspar, and quartz. Plagioclase (size: 1–3 mm) is euhedral–subhedral and polysynthetic twinned. K-feldspar (size: 0.5–4 mm) includes mainly microcline and is euhedral–subhedral and slightly kaolinite altered on the surface. The grain margins are locally rimmed by fine secondary quartz. Quartz (size: 0.8–2 mm) is euhedral granular and colorless. The microcrystalline groundmass is composed mainly of plagioclase, microcline, quartz, and minor biotite. Accessory minerals include apatite and zircon (**Figure 2C**).

The monzogranite is massive; the ores show hypidiomorphic granular texture and contain K-feldspar (35–40 vol%), plagioclase (30–35 vol%), quartz (20–25 vol%), and minor biotite (<5 vol%). K-feldspar (size: 0.5–2 mm) is euhedral–subhedral, dominated by perthite with minor microcline, and weakly kaolinite altered. Plagioclase grains (size: 0.5–3 mm) are subhedral and partially sericite and K-feldspar altered. Quartz (size: 0.7–3 mm) is anhedral granular with wavy extinction. Biotite (size: 0.4–2 mm) is flaky and chloritized locally (**Figure 2D**).

### Zircon U-Pb-Hf Isotope Analysis

Zircon grains from one porphyritic granite and one monzogranite sample were separated with conventional heavy liquid and magnetic separation techniques. LA-ICP-MS zircon U-Pb dating was completed at the State Key Laboratory of Continental Dynamics, Northwestern University. The laser ablation system used was a GeoLas 200M from MicroLas

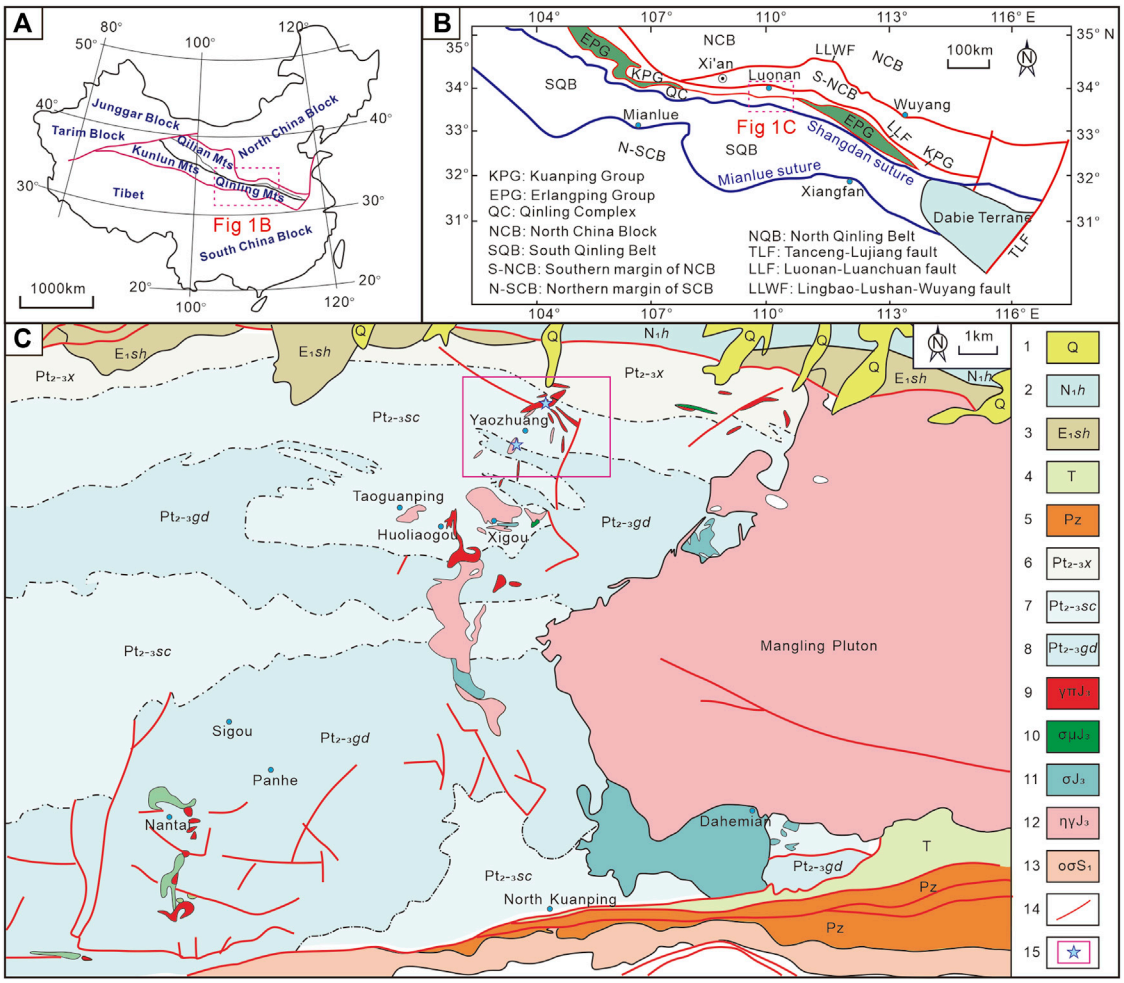


**FIGURE 1 |** Regional geological map of the western Mangling orefield [**(A)** revised after Ke et al., 2012a; **(B)** after Dong et al., 2011b].

(Germany) with a 30 μm spot size, 10 Hz repetition rate, and 32–36 MJ energy. Ion signal intensities were acquired with a quadrupole Elan 6100 DRC (ICP-MS). The instrument configuration and analytical procedures were as described by Yuan et al. (2003). Zircon GEMOC GJ-1 was used as the external standard to correct elemental fractionation and monitor instrument quality. The zircon U, Th, and Pb contents were calculated by the NIST SRM 610 glass standard (Liu et al., 2010). The method of Andersen (2002) was adopted for common Pb correction, the Glitter program (version 4.0) was used for data processing, and the Isoplot program (version 3.75) was used to calculate the U-Pb age and construct the concordia plot.

The zircon Hf isotope analysis was performed at the Laboratory of Langfang Institute of Regional Geological Survey (China), and the analysis was performed on the U-Pb dating spots. The instrument adopted the GeoLas 200M equipped with a 193 nm ArF excimer system and the Neptune plus multi-receiver plasma mass spectrometry (LA-MC-ICP-MS). The diameter of the laser ablation spot beam is 50 μm, and the denudation depth is 20–40 μm. Helium was used as the carrier gas and mixed with the argon makeup gas. The standard zircon 91500 was used as the external standard to monitor the analytical accuracy. Detailed instrumental conditions and analysis procedures were as described by Yuan et al. (2008). $^{176}Lu/^{175}Lu$ = 0.02655 and $^{176}Yb/^{172}Yb$ = 0.5887 were used for interference correction (Wu et al., 2007a).

## Whole-Rock Geochemical Analysis

Whole-rock geochemical compositions were determined at the laboratory of the #203 Institute of Nuclear Industry Geology (Xi'an, China). Major element compositions were measured with an Axios X-ray fluorescence (XRF) spectrometer (Panaco, the Netherlands). The analysis error was less than 5%. After correcting the loss on ignition (LOI), the major element oxide contents were back-calculated to 100%. Meanwhile, the standard curve was established with the GeokitPro program (Lu, 2004). The trace elements and rare Earth elements (REEs) were analyzed by the XSERIES II ICP-MS manufactured by Thermo Fisher (United States) with a precision better than 5%.

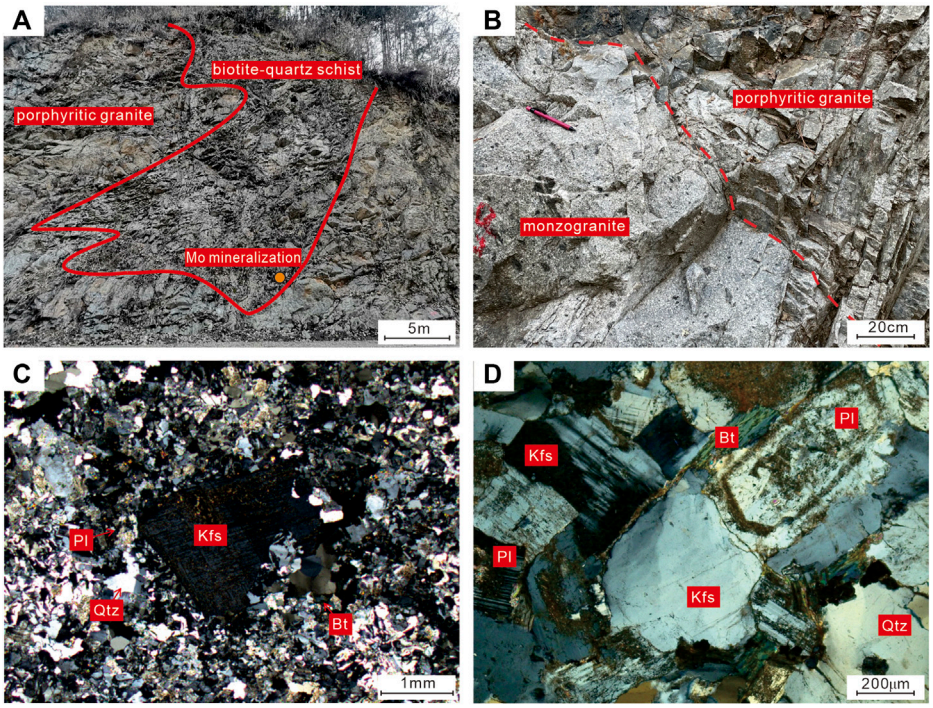


**FIGURE 2 |** Photos and microstructures of Yaozhuang stock. **(A)** Porphyritic granite intruded into biotite quartz schist; **(B)** monzogranite vein intruded into porphyritic granite; **(C)** porphyritic granite (orthogonal polarization); **(D)** monzogranite (orthogonal polarization); Kfs—K-feldspar, Pl—plagioclase, Qtz—quartz, Bt—biotite; $\gamma\pi J_3$—Late Jurassic porphyritic granite; $\eta\gamma J_3$—Late Jurassic monzogranite; $Pt_{2\text{-}3}sc$—Middle-Upper Proterozoic Sichakou rock formation.

# ANALYSIS RESULTS

## Zircon U-Pb age

The zircon grains from both samples have lengths of 70–210 μm with aspect ratios of 3:1–3:1 and are mostly transparent and euhedral elongated prismatic. CL images show clear oscillatory zoning (**Figure 3A**), with clear core–mantle–rim structures. The zircons have Th/U = 0.27–2.8, typical of magmatic zircons (Belousova et al., 2002; Wu and Zheng, 2004).

A total of 25 zircons were analyzed for porphyritic granite sample no. D92-1, among which 21 are concordant (>90%) and 17 spots fall on the concordia, yielding a weighted-mean $^{206}Pb/^{238}U$ age of 157 ± 2 Ma (MSWD = 0.15) (**Figure 3B**). A total of 25 zircons were analyzed for monzogranite sample no. D13-8, with 23 spots being concordant and 21 spots falling on the concordia, yielding a weighted-mean $^{206}Pb/^{238}U$ age of 153 ± 1 Ma (MSWD = 0.10) (**Figure 3C**). Two inherited zircons were identified, with the age of 847 ± 7 Ma. Monzogranite is slightly younger than porphyritic granite (4 Ma), consistent with the field observation that the monzogranite dike intruded the porphyritic granite (**Table 1**).

## Zircon Hf Isotope Compositions

For our two samples, their $^{176}Lu/^{177}Hf$ ratios are <0.002, indicating negligible radiogenic Hf accumulation after the zircon crystallization, and the sample $^{176}Hf/^{177}Hf$ approximates that of the entire system (Vervoort et al., 1996; Wu et al., 2007a). The samples have $f_{Lu/Hf}$ values of −0.97 to −0.94 (avg. −0.95), and $^{176}Hf/^{177}Hf$ = 0.282301–0.282485 (avg. 0.282367; porphyritic granite) and 0.282225–0.282372 (avg. 0.282317; monzogranite). The samples have $\varepsilon_{Hf}(t)$ values of −13.4 to −6.9 (porphyritic granite) and −16.1 to −11.0 (monzogranite) and two-stage Hf-isotope model ages ($t_{DM2}$) (representing the age of source material extraction from the depleted mantle) of 1.64–2.05 Ga (porphyritic granite) and 1.89–2.21 Ga (monzogranite) (**Table 2**).

## Whole-Rock Geochemistry

The major element oxide compositions of the porphyritic granite and monzogranite are similar, with $SiO_2$ = 66.83–75.63 wt%, total alkali ($Na_2O$ + $K_2O$) = 8.09–10.41 wt%, and $Al_2O_3$ = 12.90–16.93 wt%. The contents of MgO (0.06–0.73 wt%), $TFe_2O_3$ (0.99–2.23 wt%), and CaO (0.46–1.99 wt%) are generally low. The samples are high-K calc-alkaline (**Figure 4A**) and metaluminous to weakly peraluminous (A/CNK = 0.92–1.09) (**Table 3**; **Figure 4B**).

The monzogranite has a higher total REE (ΣREE = 151.4–253.6 ppm) than that of porphyritic granite (ΣREE = 139.6–161.7 ppm). Both rock types have right-inclining chondrite-normalized REE patterns (**Figure 5A**), with LREE/HREE = 14.4–25.7 and $(La/Yb)_N$ = 16.7–36.4. However, the porphyritic granite has weakly negative Eu anomalies (Eu/Eu* = 0.77–0.93), whereas the monzogranite has weakly positive Eu

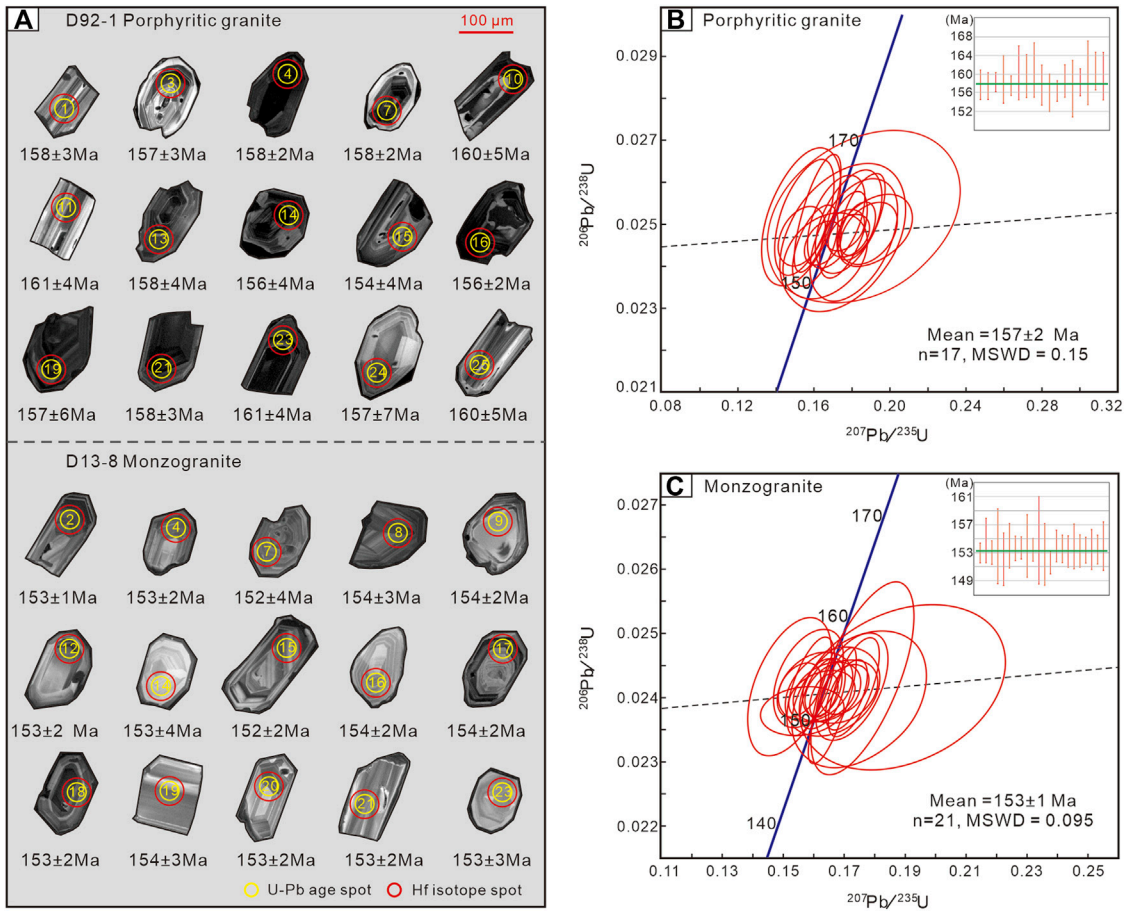


**FIGURE 3 |** Zircon CL images **(A)** and U-Pb dates **(B,C)** for Yaozhuang stock.

anomalies (Eu/Eu* = 0.97–1.21). In the primitive mantle-normalized spidergram (**Figure 5B**), both rock types are enriched in LILEs (e.g., Rb, K, and Ba) but depleted in HFSEs (e.g., Nb, Ta, Ti, Zr, and Hf) (**Table 3**).

# DISCUSSION

## Time of the Granitic Stock Emplacement

Late Mesozoic (158–112 Ma) magmatism was extensive in the North Qinling terrane (Wang et al., 2011; Liu R. et al., 2013; Lei et al., 2018; Zhang Y. S. et al., 2019; Wang et al., 2020), as represented by the Muhuguan, Mangling, and Laojunshan plutons and the nearby porphyry stocks. Recent geochronological studies had constrained the magmatic peak to be 158–144 Ma (**Table 4**), which was closely related to the regional Mo polymetallic mineralization (160–150 Ma. Mao et al., 2013, 2017). As shown in **Table 4**, the age of Mangling pluton seems to be slightly later than the stocks in the west, which may be related to the active emplacement controlled by the intersection of faults, or because the late magma in Mangling pluton may not be emplaced to the surface. In this study, the newly obtained zircon U–Pb ages for porphyritic granite (157 ± 2 Ma) and monzogranite (153 ± 1 Ma) fall within the regional magmatic peak. Combined with the available age data and features of granitic rock distribution, it constrains the magmatism of the western Mangling orefield to about 15 My.

## Petrogenesis

The Yaozhuang granitic stocks are dominantly high-K calc-alkaline and metaluminous–weakly peraluminous (0.74–1.09). The samples do not contain Al-rich minerals (e.g., garnet and corundum) that are common in S-type granites but contain sphene and apatite that are common in I-type granites. The aluminum content index (A/CNK < 1.1) indicates that they are I-type granites (Wu et al., 2007b). Combined with the data of other stocks near the study area, the Zr-10000Ga/Al diagram shows the sample plot in the I-A-type transition area (**Figure 6A**). The 160–140 Ma period is considered to be the peak period of the transformation mechanism from the paleo-Asia and Tethys tectonic domain to paleo-Pacific tectonic domain (Ding et al., 2011; Dong et al., 2018), accompanied by local crustal compression thickening and later extension. The I-A-type

**TABLE 1 |** LA-ICP-MS zircon U-Pb ages of Yaozhuang stock.

| No. | Element (ppm) | | Corrected isotope ratio | | | | | | | Apparent age (Ma) | | | | | |
|---|---|---|---|---|---|---|---|---|---|---|---|---|---|---|---|
| | Th | U | Th/U | $^{207}Pb/^{206}Pb$ | 10 | $^{207}Pb/^{235}U$ | 13 | $^{206}Pb/^{238}U$ | 13 | $^{207}Pb/^{206}Pb$ | 10 | $^{207}Pb/^{235}U$ | 13 | $^{206}Pb/^{238}U$ | 13 |
| D92-1 porphyritic granite | | | | | | | | | | | | | | | |
| 1 | 536 | 743 | 0.72 | 0.0554 | 0.0029 | 0.1883 | 0.0102 | 0.0248 | 0.0005 | 428 | 115 | 175 | 9 | 158 | 3 |
| 2 | 512 | 435 | 1.18 | 0.0502 | 0.0032 | 0.1605 | 0.0106 | 0.0231 | 0.0004 | 211 | 145 | 151 | 9 | 147 | 2 |
| 3 | 2,608 | 1,495 | 1.74 | 0.0449 | 0.0022 | 0.1532 | 0.008 | 0.0247 | 0.0005 | | | 145 | 7 | 157 | 3 |
| 4 | 1,380 | 1,566 | 0.88 | 0.0514 | 0.002 | 0.176 | 0.0068 | 0.0249 | 0.0003 | 257 | 87 | 165 | 6 | 158 | 2 |
| 5 | 667 | 796 | 0.84 | 0.0494 | 0.0022 | 0.1944 | 0.0091 | 0.0287 | 0.0008 | 165 | 138 | 180 | 8 | 182 | 5 |
| 6 | 185 | 162 | 1.15 | 0.0686 | 0.007 | 0.2313 | 0.0232 | 0.0249 | 0.0008 | 887 | 212 | 211 | 19 | 159 | 5 |
| 7 | 1,712 | 1,236 | 1.38 | 0.0524 | 0.0023 | 0.1784 | 0.007 | 0.0247 | 0.0003 | 306 | 94 | 167 | 6 | 158 | 2 |
| 8 | 429 | 605 | 0.71 | 0.0705 | 0.002 | 1.5251 | 0.0433 | 0.1567 | 0.0018 | 943 | 64 | 941 | 17 | 939 | 10 |
| 9 | 653 | 601 | 1.09 | 0.0456 | 0.0027 | 0.1549 | 0.0103 | 0.0252 | 0.0009 | | | 146 | 9 | 160 | 6 |
| 10 | 1,228 | 957 | 1.28 | 0.0495 | 0.0024 | 0.1714 | 0.01 | 0.0251 | 0.0007 | 172 | 113 | 161 | 9 | 160 | 5 |
| 11 | 1,334 | 1,234 | 1.08 | 0.048 | 0.0021 | 0.1621 | 0.0081 | 0.0253 | 0.0009 | 98 | 100 | 153 | 7 | 161 | 4 |
| 12 | 970 | 928 | 1.04 | 0.0506 | 0.0044 | 0.1861 | 0.0336 | 0.0252 | 0.0014 | 233 | 202 | 173 | 29 | 160 | 5 |
| 13 | 619 | 1,437 | 0.43 | 0.0515 | 0.0021 | 0.1757 | 0.0081 | 0.0247 | 0.0007 | 261 | 94 | 164 | 7 | 158 | 4 |
| 14 | 2,747 | 1,338 | 2.05 | 0.0483 | 0.0024 | 0.1609 | 0.0076 | 0.0245 | 0.0006 | 122 | 111 | 151 | 7 | 156 | 4 |
| 15 | 477 | 417 | 1.14 | 0.0506 | 0.0044 | 0.1661 | 0.0146 | 0.0243 | 0.0007 | 233 | 202 | 156 | 13 | 154 | 4 |
| 16 | 2,396 | 1,673 | 1.43 | 0.0487 | 0.0019 | 0.1646 | 0.0063 | 0.0246 | 0.0003 | 200 | 91 | 155 | 6 | 156 | 2 |
| 17 | 264 | 673 | 0.39 | 0.1088 | 0.0024 | 4.4053 | 0.116 | 0.2936 | 0.0049 | 1780 | 41 | 1,713 | 22 | 1,659 | 24 |
| 18 | 526 | 371 | 1.42 | 0.0561 | 0.0037 | 0.1923 | 0.013 | 0.0249 | 0.0006 | 457 | 146 | 179 | 11 | 159 | 3 |
| 19 | 269 | 985 | 0.27 | 0.053 | 0.0035 | 0.1811 | 0.0152 | 0.0246 | 0.001 | 328 | 150 | 169 | 13 | 157 | 6 |
| 20 | 986 | 554 | 1.78 | 0.079 | 0.0091 | 0.2865 | 0.0486 | 0.0247 | 0.001 | 1,172 | 231 | 256 | 38 | 157 | 6 |
| 21 | 2,876 | 2,218 | 1.3 | 0.0533 | 0.002 | 0.1821 | 0.0067 | 0.0248 | 0.0005 | 339 | 83 | 170 | 6 | 158 | 3 |
| 22 | 606 | 406 | 1.49 | 0.0465 | 0.0046 | 0.1532 | 0.0136 | 0.0252 | 0.0011 | 33 | 222 | 145 | 12 | 160 | 7 |
| 23 | 2,131 | 1,907 | 1.12 | 0.0535 | 0.0022 | 0.1855 | 0.008 | 0.0252 | 0.0006 | 350 | 93 | 173 | 7 | 161 | 4 |
| 24 | 434 | 285 | 1.52 | 0.0496 | 0.004 | 0.1753 | 0.0218 | 0.0247 | 0.0012 | 176 | 191 | 164 | 19 | 157 | 7 |
| 25 | 498 | 457 | 1.09 | 0.053 | 0.0035 | 0.1784 | 0.0116 | 0.0251 | 0.0008 | 332 | 150 | 167 | 10 | 160 | 5 |
| D13-8 monzogranite | | | | | | | | | | | | | | | |
| 1 | 251 | 422 | 0.59 | 0.0701 | 0.0015 | 1.43 | 0.0326 | 0.1476 | 0.0016 | 931 | 43 | 902 | 14 | 888 | 9 |
| 2 | 4,102 | 1,464 | 2.8 | 0.0492 | 0.001 | 0.1632 | 0.0031 | 0.024 | 0.0002 | 167 | 42 | 153 | 3 | 153 | 1 |
| 3 | 438 | 960 | 0.46 | 0.0491 | 0.0027 | 0.1583 | 0.0076 | 0.0243 | 0.0005 | 154 | 130 | 149 | 7 | 155 | 3 |
| 4 | 587 | 509 | 1.15 | 0.0492 | 0.0022 | 0.1628 | 0.0071 | 0.024 | 0.0003 | 167 | 101 | 153 | 6 | 153 | 2 |
| 5 | 127 | 409 | 0.31 | 0.0663 | 0.0013 | 1.2166 | 0.0212 | 0.1331 | 0.001 | 817 | 39 | 808 | 10 | 805 | 6 |
| 6 | 139 | 174 | 0.8 | 0.0563 | 0.0052 | 0.1891 | 0.0223 | 0.0242 | 0.0008 | 465 | 202 | 176 | 19 | 154 | 5 |
| 7 | 398 | 932 | 0.43 | 0.0505 | 0.0014 | 0.1662 | 0.0052 | 0.0239 | 0.0006 | 220 | 56 | 156 | 5 | 152 | 4 |
| 8 | 906 | 507 | 1.79 | 0.048 | 0.0018 | 0.159 | 0.0051 | 0.0242 | 0.0005 | 98 | 87 | 150 | 5 | 154 | 3 |
| 9 | 773 | 952 | 0.81 | 0.0467 | 0.0015 | 0.1551 | 0.0047 | 0.0241 | 0.0003 | 35 | 87 | 146 | 4 | 154 | 2 |
| 10 | 292 | 869 | 0.34 | 0.0513 | 0.0017 | 0.1703 | 0.0052 | 0.0241 | 0.0003 | 254 | 76 | 160 | 4 | 154 | 2 |
| 11 | 384 | 261 | 1.47 | 0.0457 | 0.0026 | 0.1521 | 0.0091 | 0.0242 | 0.0007 | | | 144 | 8 | 154 | 4 |
| 12 | 1,518 | 1,013 | 1.5 | 0.0493 | 0.0014 | 0.1635 | 0.0045 | 0.0241 | 0.0003 | 167 | 69 | 154 | 4 | 153 | 2 |
| 13 | 337 | 1,144 | 0.3 | 0.0518 | 0.0013 | 0.176 | 0.0111 | 0.0243 | 0.001 | 280 | 62 | 165 | 10 | 155 | 6 |
| 14 | 64 | 98 | 0.66 | 0.0539 | 0.0049 | 0.175 | 0.0146 | 0.024 | 0.0007 | 365 | 210 | 164 | 13 | 153 | 4 |
| 15 | 403 | 319 | 1.26 | 0.048 | 0.0031 | 0.1561 | 0.0091 | 0.0238 | 0.0003 | 102 | 154 | 147 | 8 | 152 | 2 |
| 16 | 463 | 394 | 1.17 | 0.048 | 0.0022 | 0.1605 | 0.0081 | 0.0242 | 0.0004 | 98 | 113 | 151 | 7 | 154 | 2 |
| 17 | 679 | 1,658 | 0.41 | 0.049 | 0.0012 | 0.1626 | 0.0037 | 0.0241 | 0.0003 | 146 | 56 | 153 | 3 | 154 | 2 |
| 18 | 2,023 | 1,840 | 1.1 | 0.0516 | 0.0013 | 0.1707 | 0.0045 | 0.024 | 0.0004 | 265 | 59 | 160 | 4 | 153 | 2 |
| 19 | 1,617 | 728 | 2.22 | 0.0522 | 0.0018 | 0.1731 | 0.0056 | 0.0242 | 0.0005 | 295 | 80 | 162 | 5 | 154 | 3 |
| 20 | 2,631 | 1,500 | 1.75 | 0.0491 | 0.0012 | 0.1628 | 0.0046 | 0.0241 | 0.0004 | 150 | 55 | 153 | 4 | 153 | 2 |
| 21 | 1,120 | 768 | 1.46 | 0.05 | 0.0017 | 0.1662 | 0.006 | 0.0241 | 0.0003 | 195 | 106 | 156 | 5 | 153 | 2 |
| 22 | 145 | 534 | 0.27 | 0.1625 | 0.0025 | 3.9755 | 0.2317 | 0.1765 | 0.0094 | 2,483 | 26 | 1,629 | 47 | 1,048 | 52 |
| 23 | 197 | 173 | 1.14 | 0.05 | 0.0031 | 0.1662 | 0.0104 | 0.0241 | 0.0005 | 195 | 151 | 156 | 9 | 153 | 3 |
| 24 | 451 | 452 | 1 | 0.051 | 0.0023 | 0.1692 | 0.0079 | 0.0241 | 0.0003 | 239 | 106 | 159 | 7 | 153 | 2 |
| 25 | 1,261 | 754 | 1.67 | 0.052 | 0.0025 | 0.1724 | 0.0079 | 0.0242 | 0.0006 | 287 | 111 | 161 | 7 | 154 | 3 |

transition granites are just the products of this period. The ($K_2O$ + $Na_2O$)/CaO vs. (Zr + Nb + Ce + Y) diagram shows the features of high-fractionation granites (**Figure 6B**). The occurrence of high-fractionation granites is mainly related to high-temperature magma and rich volatiles, while fractionated crystallization often occurs in emplacement along with extensional structures (Wu et al., 2017). Interestingly, highly fractionated crystallization is of great significance for the enrichment of rare metal minerals (Xu et al., 2021).

Zircon U-Pb age and Hf isotopes can effectively constrain the magma source and crustal evolution (Kinny and Roland, 2003; Xu et al., 2004; Kemp et al., 2007). The similar REEs and trace

**TABLE 2 |** Zircon Lu-Hf isotope results in Yaozhuang stock.

| No. | Age (Ma) | $^{176}Hf/^{177}Hf$ | 2σ | $^{176}Yb/^{177}Hf$ | 2σ | $^{176}Lu/^{177}Hf$ | 2σ | $I_{Hf}$ | εHf | $T_{DM}$ (Ma) | $T_{DM2}$ (Ma) | *fLu/Hf* |
|---|---|---|---|---|---|---|---|---|---|---|---|---|
| D92-1 porphyritic granite | | | | | | | | | | | | |
| D92-1-01 | 158 | 0.282341 | 0.00002 | 0.08896 | 0.00078 | 0.00202 | 0.00002 | 0.282335 | −12 | 1,321 | 1,956 | −0.94 |
| D92-1-03 | 157 | 0.282363 | 0.00002 | 0.07857 | 0.001 | 0.00187 | 0.00002 | 0.282358 | −11.2 | 1,285 | 1,907 | −0.94 |
| D92-1-06 | 159 | 0.282485 | 0.00003 | 0.08048 | 0.00197 | 0.00196 | 0.00005 | 0.282479 | −6.9 | 1,112 | 1,637 | −0.94 |
| D92-1-07 | 158 | 0.28238 | 0.00003 | 0.06288 | 0.00131 | 0.00161 | 0.00002 | 0.282375 | −10.6 | 1,252 | 1,868 | −0.95 |
| D92-1-13 | 158 | 0.282367 | 0.00002 | 0.0683 | 0.00016 | 0.00172 | 0 | 0.282362 | −11 | 1,274 | 1,898 | −0.95 |
| D92-1-14 | 158 | 0.282374 | 0.00002 | 0.07421 | 0.00322 | 0.00168 | 0.00007 | 0.282369 | −10.8 | 1,263 | 1,882 | −0.95 |
| D92-1-18 | 158 | 0.282413 | 0.00002 | 0.08681 | 0.00013 | 0.00198 | 0 | 0.282407 | −9.4 | 1,217 | 1,798 | −0.94 |
| D92-1-19 | 157 | 0.282303 | 0.00002 | 0.05378 | 0.00017 | 0.00137 | 0 | 0.282299 | −13.3 | 1,352 | 2,036 | −0.96 |
| D92-1-21 | 157 | 0.282301 | 0.00002 | 0.08457 | 0.00119 | 0.00182 | 0.00003 | 0.282295 | −13.4 | 1,373 | 2,045 | −0.95 |
| D92-1-24 | 160 | 0.282345 | 0.00003 | 0.08197 | 0.00257 | 0.00193 | 0.00006 | 0.282339 | −11.8 | 1,313 | 1,946 | −0.94 |
| D13-8 monzogranite | | | | | | | | | | | | |
| D13-8-04 | 153 | 0.282291 | 0.00003 | 0.06485 | 0.00114 | 0.00179 | 0.00002 | 0.282286 | −13.8 | 1,385 | 2,068 | −0.95 |
| D13-8-07 | 152 | 0.282346 | 0.00002 | 0.07015 | 0.00035 | 0.0018 | 0.00001 | 0.282341 | −11.9 | 1,307 | 1,948 | −0.95 |
| D13-8-08 | 154 | 0.282372 | 0.00003 | 0.06953 | 0.00451 | 0.00172 | 0.00011 | 0.282367 | −11 | 1,267 | 1,889 | −0.95 |
| D13-8-09 | 154 | 0.28231 | 0.00003 | 0.06009 | 0.00194 | 0.00166 | 0.00005 | 0.282306 | −13.1 | 1,353 | 2,024 | −0.95 |
| D13-8-10 | 154 | 0.282225 | 0.00002 | 0.04428 | 0.00037 | 0.00107 | 0.00001 | 0.282222 | −16.1 | 1,451 | 2,209 | −0.97 |
| D13-8-12 | 154 | 0.282361 | 0.00003 | 0.07157 | 0.00016 | 0.00186 | 0.00001 | 0.282356 | −11.3 | 1,288 | 1,914 | −0.94 |
| D13-8-13 | 155 | 0.282288 | 0.00002 | 0.06579 | 0.00059 | 0.00186 | 0.00001 | 0.282282 | −13.9 | 1,392 | 2,075 | −0.94 |
| D13-8-14 | 153 | 0.282359 | 0.00003 | 0.04588 | 0.00011 | 0.00116 | 0 | 0.282355 | −11.4 | 1,267 | 1,915 | −0.97 |
| D13-8-16 | 154 | 0.282312 | 0.00002 | 0.09271 | 0.00052 | 0.00199 | 0.00002 | 0.282306 | −13.1 | 1,362 | 2,022 | −0.94 |
| D13-8-17 | 154 | 0.282301 | 0.00002 | 0.06552 | 0.00022 | 0.00182 | 0.00001 | 0.282296 | −13.5 | 1,372 | 2,046 | −0.95 |
| D13-8-23 | 153 | 0.282346 | 0.00002 | 0.09296 | 0.00103 | 0.0019 | 0.00003 | 0.28234 | −11.9 | 1,311 | 1,948 | −0.94 |
| D13-8-24 | 153 | 0.282297 | 0.00002 | 0.08451 | 0.00034 | 0.00187 | 0.00001 | 0.282291 | −13.7 | 1,380 | 2,056 | −0.94 |

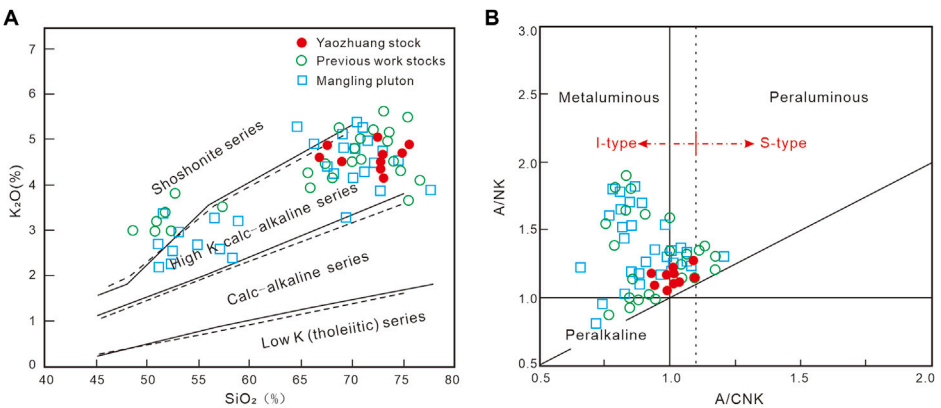


**FIGURE 4 |** Plots of $SiO_2$ vs. $K_2O$ [**(A)** after Peccerillo and Taylor, 1976) and A/CNK vs A/NK **(B)** after Maniar and Piccoli, 1989] of the Yaozhuang stock (previous work stocks data after Ke et al., 2012a; Qin et al., 2012; Yang et al., 2014; Hu et al., 2017; Zhang Y. S. et al., 2019).

element patterns (**Figure 5**) and zircon $\varepsilon_{Hf}(t)$ values of the porphyritic granite and monzogranite suggest a common magma source. The $\varepsilon_{Hf}(t)$ values of crystalline zircons range from −16.1 to −6.9, and the sample points are located near the evolution line of the lower crust (**Figures 7A,B**). The $\varepsilon_{Hf}(t)$–t and La–La/Sm diagrams (**Figure 8A**) show the source mainly originates from partial melting of the lower crust. Moreover, Ke et al. (2012b) found that the Xigou stock at the western Mangling pluton had low $\varepsilon_{Hf}(t)$ values (−8.9 to −0.8), which implied that some mantle-derived components may be mixed into the lower crustal melt. A small number of mafic dikes [e.g., lamprophyre dikes of Muhuguan (152 ± 1 Ma) and gabbro dikes of Mokou (145 ± 2 Ma, 132 ± 3 Ma)] also indicates the addition of mantle-derived components (Liu et al., 2013; Liang et al., 2020). The $Mg^{\#}$ [atomic Mg/(Mg + Fe) × 100] values of lower crustal melts are usually below 40, and thus, $Mg^{\#} > 40$ often indicates mantle material involvement (Wilson, 1989; Kelemen, 1995; Smithies and Champion, 2000). The $Mg^{\#}$ values of our samples (33–77, avg. 61) suggest mantle input in the magma source region.

The fractional crystallization of garnet leads to a significant increase in the ratios of $(La/Yb)_N$ and $(Dy/Yb)_N$ (Blundy and Wood, 1994; He et al., 2011). The separation crystallization of garnet (or as a residual phase in the source

**TABLE 3 |** The major elements (wt%) and trace elements (ppm) of Yaozhuang stock.

| Sample | D91-1 | D91-2 | D92-1 | D92-2 | D92-3 | D13-2 | D13-3 | D13-5 | D13-7 | D13-8 |
|---|---|---|---|---|---|---|---|---|---|---|
| Lithology | Porphyritic granite | | | | | Monzogranite | | | | |
| $SiO_2$ | 75.63 | 74.96 | 72.91 | 72.89 | 73.14 | 67.63 | 66.83 | 72.52 | 73.02 | 69.03 |
| $Al_2O_3$ | 12.90 | 13.19 | 13.65 | 13.64 | 14.10 | 16.61 | 16.93 | 14.02 | 13.38 | 15.19 |
| $TFe_2O_3$ | 0.99 | 1.22 | 1.61 | 1.56 | 1.50 | 2.03 | 2.23 | 1.60 | 1.84 | 2.22 |
| MgO | 0.06 | 0.23 | 0.73 | 0.52 | 0.37 | 0.46 | 0.59 | 0.50 | 0.42 | 0.73 |
| CaO | 0.49 | 0.63 | 1.15 | 1.11 | 1.09 | 0.46 | 1.66 | 0.60 | 1.14 | 1.99 |
| $Na_2O$ | 4.17 | 4.11 | 4.11 | 4.21 | 3.94 | 5.53 | 5.33 | 4.26 | 4.34 | 4.80 |
| $K_2O$ | 4.89 | 4.71 | 4.52 | 4.35 | 4.15 | 4.88 | 4.61 | 5.05 | 4.66 | 4.52 |
| $P_2O_5$ | 0.04 | 0.02 | 0.06 | 0.07 | 0.07 | 0.08 | 0.09 | 0.06 | 0.05 | 0.11 |
| MnO | 0.04 | 0.07 | 0.08 | 0.09 | 0.08 | 0.05 | 0.09 | 0.06 | 0.04 | 0.09 |
| $TiO_2$ | 0.11 | 0.16 | 0.19 | 0.19 | 0.18 | 0.29 | 0.27 | 0.21 | 0.20 | 0.30 |
| LOI | 0.42 | 0.59 | 0.68 | 1.08 | 1.03 | 1.58 | 1.09 | 1.14 | 0.87 | 0.79 |
| Total | 99.74 | 99.89 | 99.69 | 99.71 | 99.65 | 99.60 | 99.72 | 100.02 | 99.96 | 99.77 |
| Mg# | 33 | 59 | 77 | 68 | 57 | 74 | 69 | 74 | 62 | 68 |
| A/CNK | 0.99 | 1.01 | 0.99 | 1.00 | 1.09 | 1.09 | 1.01 | 1.03 | 0.94 | 0.92 |
| La | 42.62 | 38.27 | 36.49 | 37.81 | 44.24 | 58.25 | 46.70 | 39.11 | 40.43 | 60.66 |
| Ce | 61.37 | 63.82 | 63.40 | 63.37 | 72.68 | 131.91 | 140.52 | 71.78 | 67.33 | 95.32 |
| Pr | 7.18 | 6.90 | 6.35 | 6.57 | 7.41 | 12.30 | 13.20 | 7.33 | 7.22 | 9.78 |
| Nd | 22.60 | 21.41 | 20.27 | 21.13 | 23.42 | 34.97 | 37.74 | 23.62 | 22.90 | 30.71 |
| Sm | 3.59 | 3.10 | 3.19 | 3.34 | 3.61 | 3.77 | 3.85 | 3.61 | 3.38 | 4.13 |
| Eu | 0.82 | 0.89 | 0.90 | 0.92 | 1.00 | 1.46 | 1.68 | 1.17 | 1.04 | 1.51 |
| Gd | 2.99 | 3.04 | 2.77 | 2.93 | 3.19 | 4.48 | 4.65 | 3.43 | 3.16 | 4.27 |
| Tb | 0.41 | 0.38 | 0.37 | 0.38 | 0.40 | 0.38 | 0.41 | 0.42 | 0.40 | 0.48 |
| Dy | 2.20 | 2.11 | 2.04 | 2.00 | 2.10 | 1.76 | 1.97 | 2.49 | 2.13 | 2.46 |
| Ho | 0.46 | 0.38 | 0.43 | 0.42 | 0.44 | 0.34 | 0.37 | 0.47 | 0.41 | 0.46 |
| Er | 1.39 | 1.33 | 1.28 | 1.22 | 1.33 | 1.05 | 1.10 | 1.37 | 1.20 | 1.38 |
| Tm | 0.24 | 0.20 | 0.22 | 0.22 | 0.22 | 0.17 | 0.18 | 0.22 | 0.20 | 0.22 |
| Yb | 1.65 | 1.44 | 1.57 | 1.45 | 1.49 | 1.08 | 1.12 | 1.48 | 1.42 | 1.55 |
| Lu | 0.26 | 0.24 | 0.25 | 0.24 | 0.24 | 0.18 | 0.19 | 0.24 | 0.24 | 0.26 |
| Y | 13.11 | 13.24 | 12.28 | 11.70 | 13.22 | 10.39 | 11.78 | 15.33 | 13.89 | 15.90 |
| Rb | 177.3 | 159.7 | 175.6 | 168.4 | 163.5 | 156.0 | 138.2 | 157.2 | 131.9 | 144.2 |
| Ba | 815.5 | 1,007.4 | 1,043.0 | 984.5 | 1,054.0 | 835.4 | 682.8 | 940.4 | 1,120.0 | 948.5 |
| Th | 22.44 | 19.77 | 20.61 | 19.43 | 20.46 | 16.02 | 16.21 | 19.58 | 21.23 | 20.04 |
| U | 4.25 | 3.48 | 4.21 | 3.18 | 2.33 | 1.47 | 2.74 | 2.19 | 9.46 | 5.27 |
| Nb | 35.45 | 21.73 | 24.29 | 23.06 | 23.01 | 11.58 | 9.67 | 18.81 | 20.56 | 16.71 |
| Ta | 2.86 | 1.75 | 2.12 | 2.14 | 2.14 | 0.41 | 0.58 | 1.48 | 1.64 | 1.34 |
| Sr | 85.7 | 106.4 | 124.7 | 120.9 | 128.2 | 238.0 | 518.6 | 166.3 | 179.3 | 409.7 |
| Hf | 5.05 | 4.14 | 4.35 | 4.62 | 5.26 | 8.01 | 7.50 | 4.52 | 4.94 | 6.43 |
| Zr | 113.7 | 129.4 | 121.7 | 121.9 | 156.2 | 364.2 | 351.8 | 144.3 | 159.5 | 250.6 |
| Ga | 16.57 | 17.63 | 16.71 | 16.78 | 17.84 | 19.80 | 21.48 | 18.12 | 18.07 | 19.49 |
| Sc | 3.81 | 3.63 | 4.31 | 4.24 | 4.40 | 3.88 | 3.73 | 3.82 | 3.94 | 4.65 |
| Cr | 13.67 | 11.02 | 9.29 | 9.45 | 12.50 | 17.03 | 19.89 | 14.75 | 19.21 | 16.48 |
| Co | 1.04 | 1.20 | 1.76 | 1.61 | 2.34 | 3.19 | 3.19 | 2.26 | 2.27 | 3.81 |
| Ni | 3.53 | 3.08 | 4.50 | 4.86 | 5.35 | 7.35 | 8.40 | 6.46 | 6.74 | 6.93 |
| ∑REE | 147.8 | 143.5 | 139.6 | 142.0 | 161.7 | 252.2 | 253.6 | 156.7 | 151.4 | 213.2 |
| LREE/HREE | 14.39 | 14.74 | 14.63 | 15.03 | 16.19 | 25.70 | 24.40 | 14.49 | 15.53 | 18.24 |
| (La/Yb)N | 18.52 | 19.08 | 16.68 | 18.70 | 21.28 | 36.42 | 28.14 | 18.95 | 20.41 | 28.09 |
| Eu/Eu* | 0.77 | 0.89 | 0.93 | 0.90 | 0.90 | 1.09 | 1.21 | 1.02 | 0.97 | 1.10 |

area) and the inconspicuous Eu anomaly are usually interpreted as deeper crustal melting (Rudnick and Gao, 2003; Zhang et al., 2018). Yaozhuang stock shows positive correlation on $(La/Yb)_N$ and $(Dy/Yb)_N$ (**Figure 8B**). When the depth of the magma source area is >40 km and the pressure is >1.0–1.2 GPa, garnet will exist as the residual face in the magma source area (Rapp et al., 1999). Therefore, it is speculated that Yaozhuang granitic magma comes from the deep source region >40 km.

## Tectonic Implications

The magmatism in the North Qinling terrane is still debated. Some workers suggested that magmatism occurred after the collision of the North China Plate and the Yangtze Plate (Zhu et al., 2009, 2010; Dong et al., 2013), while others inferred that it was caused by the far-field tectonic transition effect of the Paleo-Pacific subduction beneath the Eurasia plate (Wang et al., 2015; Gao and Zhao., 2017; Yang et al., 2021). The Qinling orogen may have undergone continent–continent

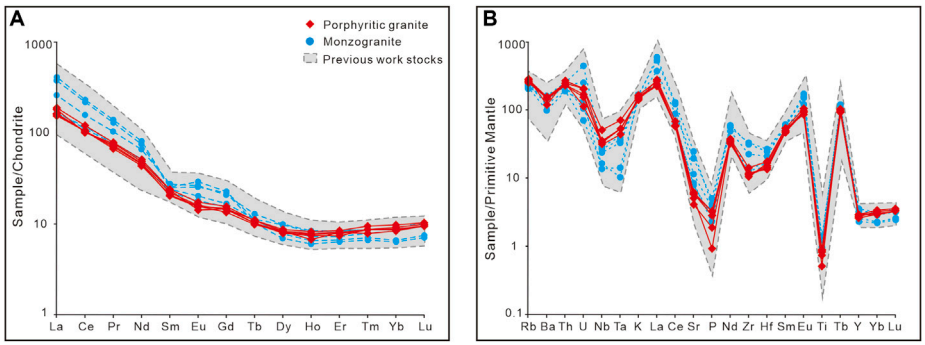


**FIGURE 5 |** Chondrite-normalized REE patterns **(A)** and primitive mantle-normalized spidergram **(B)** of Yaozhuang stock (normalized values after Sun and McDonough, 1989; previous work stocks data after Ke et al., 2012a; Qin et al., 2012; Yang et al., 2014; Hu et al., 2017; Zhang Y. S. et al., 2019).

**TABLE 4 |** Age statistics of granitic batholith and stocks in the North Qinling.

| Type | Research object | Chronological method | Age (Ma) | Data sources |
|---|---|---|---|---|
| Stocks | Taoguanping monzogranite | LA-ICP-MS Zircon U-Pb | 157±1 | Ke et al. (2012) |
| | Xigou monzogranite | LA-ICP-MS Zircon U-Pb | 153±1 | Ke et al. (2012) |
| | Nantai granite porphyry | LA-ICP-MS Zircon U-Pb | 151±1 | Ke et al. (2014) |
| | Muhuguan lamprophyre dike | LA-ICP-MS Zircon U-Pb | 152±1 | Liu R. et al. (2013) |
| | Mokou lamprophyre dike | LA-ICP-MS Zircon U-Pb | 147±3 | Liang et al. (2020) |
| | Yaozhuang porphyroid granite | LA-ICP-MS Zircon U-Pb | 157±2 | This study |
| | Yaozhuang monzogranite | LA-ICP-MS Zircon U-Pb | 153±1 | This study |
| Plutons | Mangling biotite diorite | LA-ICP-MS Zircon U-Pb | 157±1 | Yang et al. (2014) |
| | Mangling porphyroid biotite monzogranite | LA-ICP-MS Zircon U-Pb | 148±1 | Yang et al. (2014) |
| | Mangling medium-grained monzogranite | LA-ICP-MS Zircon U-Pb | 144±1 | Yang et al. (2014) |
| | Mangling K-feldspar granite | LA-ICP-MS Zircon U-Pb | 124±2 | Qin et al. (2012) |
| | Muhuguan monzogranite | LA-ICP-MS Zircon U-Pb | 145±3 | Zhang Y. S. et al. (2019) |
| | Muhuguan dark enclaves (MMEs) | LA-ICP-MS Zircon U-Pb | 152±1 | Liu R. et al. (2013) |
| | Laojunshan biotite monzogranite | SHRIMP Zircon U-Pb | 111±1 | Meng et al. (2012) |

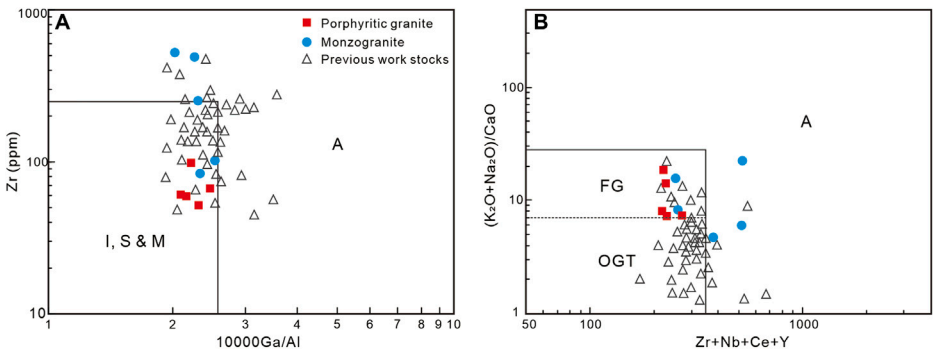


**FIGURE 6 |** Zr-10000Ga/Al diagram [**(A)** after Joseph et al., 1987] and ($K_2O$ + $Na_2O$)/CaO-Zr + Nb + Ce + Y diagram [**(B)** after Joseph et al., 1987; previous work stocks data after Ke et al., 2012a; Qin et al., 2012; Yang et al., 2014; Hu et al., 2017; Zhang Y. S. et al., 2019].

collision in the Middle-Late Triassic (242–221 Ma), followed by an intraplate orogenic stage (Bao et al., 2015; Li et al., 2015; Chen et al., 2019). In the Late Triassic (220–195 Ma), it was the late syncollision or post-collision tectonic environment. Some alkaline syenites, rapakivi granites, and I-type granites are developed in the region (Dong et al., 2011a; 2011b; Ding et al., 2011; Wang et al., 2013), followed by tectonic quiescence in the early Middle Jurassic (195–160 Ma) (Li N. et al., 2018). In the Late Jurassic (160–140 Ma), there are some bimodal magmatism, mafic microgranular enclaves, and lamprophyre dikes in the Qinling orogeny (Wang et al., 2008; Liang et al., 2020), implying that

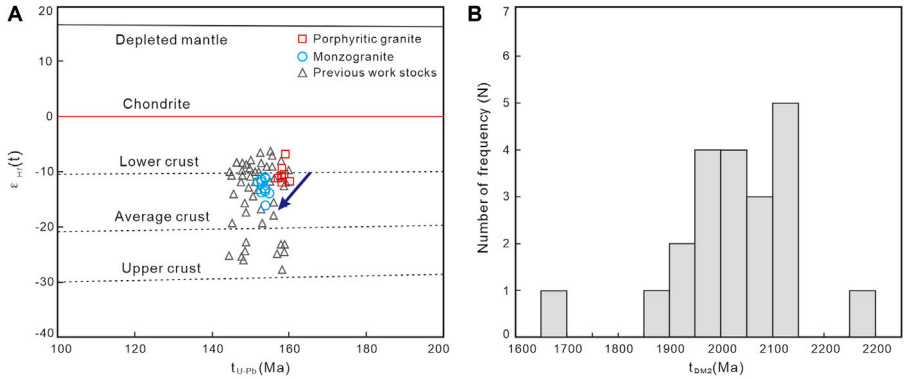


**FIGURE 7 |** Zircon $\varepsilon_{Hf}(t)$-t diagram of Yaozhuang stock **(A)** and $t_{DM2}$ statistical histogram **(B)** (data after Dong et al., 2011a; Ke et al., 2012b; Liu et al., 2014; Zhao et al., 2021).

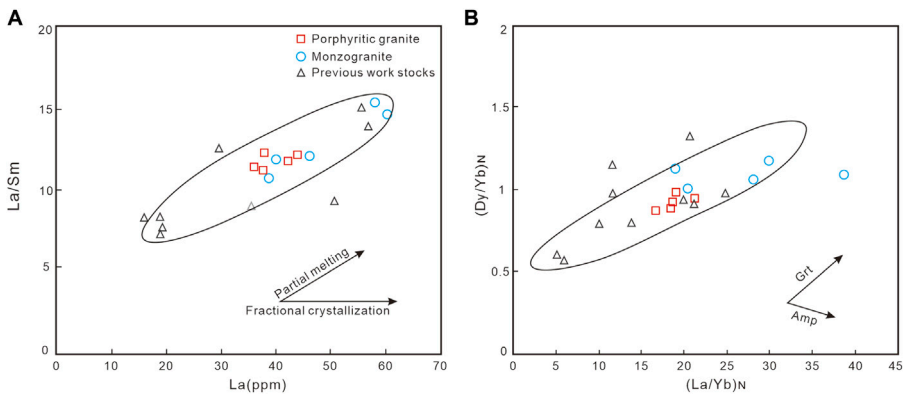


**FIGURE 8 |** La-La/Sm diagram **(A)** and $(La/Yb)_N$ vs $(Dy/Yb)_N$ diagram **(B)** of Yaozhuang stocks and [**(A,B)** after He et al., 2011; data after Ke et al., 2012a].

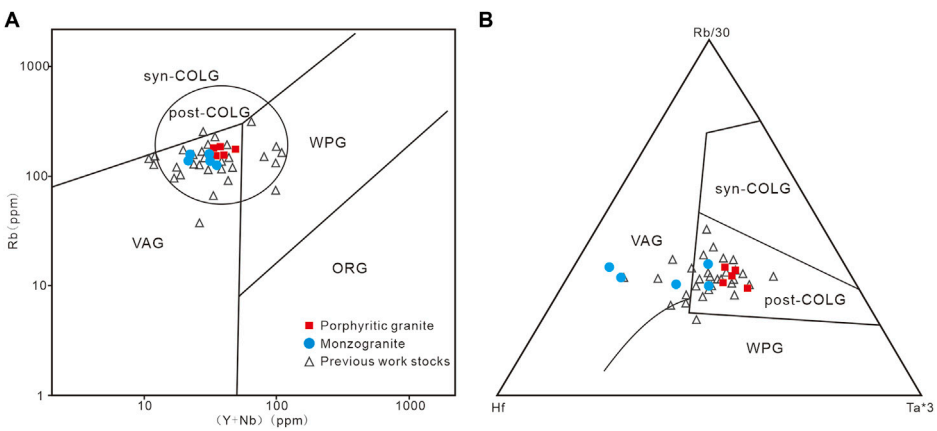


**FIGURE 9 |** Rb-(Y + Nb) plot [**(A)** after Pearce, 1996] and Hf-Rb/30-Ta*3 plot [**(B)** after Harris et al., 1986] of Yaozhuang stock.

lithospheric extension may have occurred (Liu et al., 2013). Both the Rb vs. (Y + Nb) and Hf-Rb/30-Ta*3 diagrams also revealed post-collisional magmatism (**Figures 9A,B**).

Geophysical data show that there was a WNW-directed uplift in the southern margin of the North China Craton (Xu et al., 2004, 2009; Zhou 2006), which is consistent

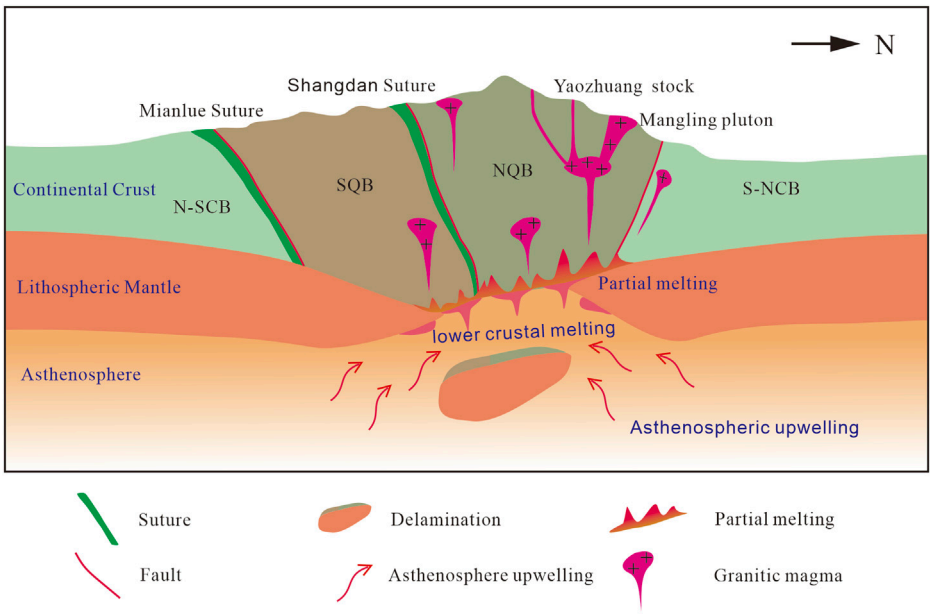


**FIGURE 10 |** Tectonic magmatic model map of the North Qinling.

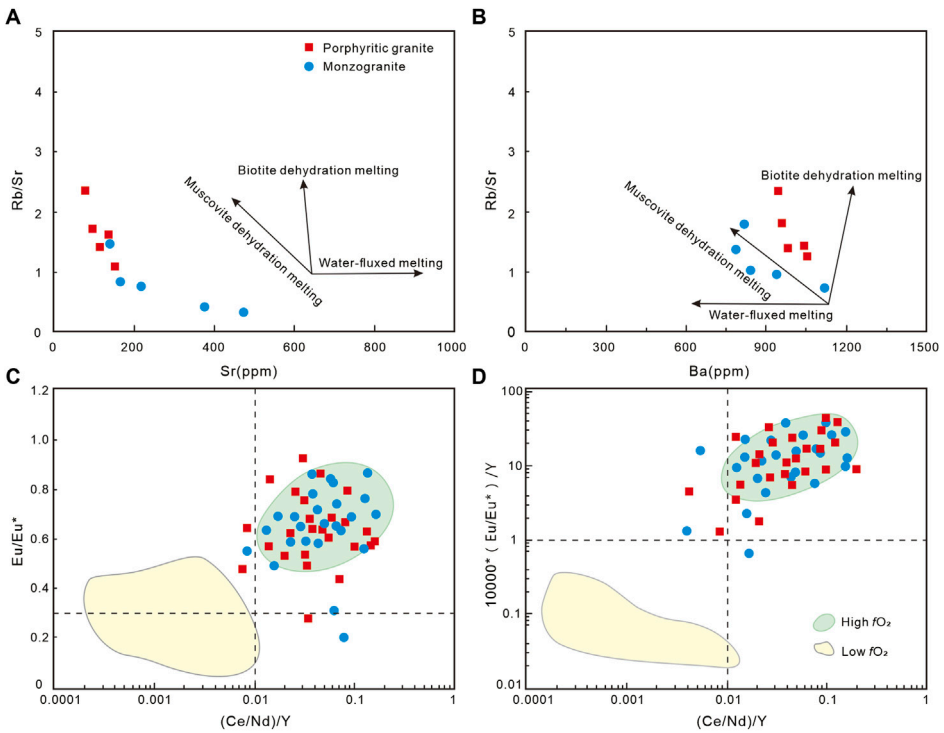


**FIGURE 11 |** Sr vs. Rb/Sr diagram [**(A)** after Inger and Harris, 1993], Ba vs. Rb/Sr diagram [**(B)** after Inger and Harris, 1993], 10,000*(Eu/Eu*)/Y vs. (Ce/Nd)/Y **(C)**, and (Eu/Eu*)/Y vs. (Ce/Nd)/Y **(D)** plots for zircons from Yaozhuang stock [**(C,D)** after Lu et al., 2016].

with the large Qinling Mo ore belt, regional deep faults and widespread pluton emplacement in the Late Mesozoic. All indicate that the mantle upwelling may occur in the North Qinling terrane. Underplating melting has provided the heat and material for the coeval magmatism.

Some workers suggested a flat-slab subduction model that the Paleo-Pacific subduction could extend up to 1,300 km inland and cause large-scale magmatism in the Late Mesozoic (Li and Li., 2007; Gao and Zhao., 2017). Zhou (2006) argues that the gravity gradient and lithosphere thickness of the Qinling orogen decreases from south to north, but the gravity gradient and lithospheric thickness in eastern China decrease from west to east and cross with the Qinling orogenic belt. If affected by the Paleo-Pacific subduction, the variation of gravity gradient and lithospheric thickness should be consistent in the NE direction, and a large number of NE-trending magmatism should be found. However, the late Mesozoic magmatism in the Qinling area is nearly E–W in direction. We suggest that the Paleo-Pacific subduction has a limited impact on North Qinling, but a significant impact on the decratonization in North China. The study area is about 1,700 km far away from the Paleo-Pacific subduction zone and should have a negligible impact on the subduction. Therefore, regional tectonics may have been controlled mainly by the collision orogeny. We propose that in the North Qinling terrane, the asthenospheric materials may have upwelled and heated the lithospheric mantle to form mantle-derived magma. Subsequently, the magma underplating may have triggered partial melting of the lower crust, and the resultant magma may have then evolved and fractionated. Finally, the highly fractionated granitic magmas may have intruded into the intersection of the older EW-trending faults and the younger NE-trending faults (**Figure 10**).

## Implications for Mo Polymetallic Ore Prospecting

The formation of porphyry Mo deposits is controlled by many factors, including the content of water and sulfur in magmatic–hydrothermal solution, oxygen fugacity of magma (Burnham and Berry, 2012), and the migration of metal elements (Sillitoe, 2010; Richards et al., 2012; Park et al., 2021). Porphyry metallogenic magmas not only in subduction settings but also in collision settings have significant water-rich (>4.0%) (Wang et al., 2014a) and high-oxygen fugacity (Delta FMQ > 1.5) (Richards, 2011; Wang et al., 2014b). Previous studies have found that the separation and crystallization of amphibole from the magmatic system require a high water content (4%) (Naney, 1983; Davidson et al., 2007; Ridolfi et al., 2010), but the high water content will inhibit the separation and crystallization of plagioclase (Wang et al., 2021), so that the rare Earth element distribution model of water-rich magma does not show Eu anomaly. The Eu of the studied stock shows no or weakly negative anomalies (Eu/Eu* = 0.77–1.21, avg. 0.98). Moreover, some contemporaneous diorite rocks are found near the study area, containing a large number of amphibole cumulates (Liu et al., 2014; Yang et al., 2014). These characteristics suggest that the original magma has high water content ($H_2O$ > 4%).

Inger and Harris (1993) found that the dehydration and melting of muscovite would lead to the increase of the Rb/Sr ratio and the decrease of Sr and Ba contents in the melt; the trend diagram of dehydration melting and water-fluxed melting was divided (Sylvester, 1998; Meng et al., 2021). From **Figures 11A,B**, it is seen that the Yaozhuang stock shows a good trend of Muscovite dehydration melting; the fluid formed by dehydration melting of water-bearing minerals in the crust leads to further melting of the rock (Weinberg and Hasalová, 2015). Generally, the melt formed by dehydration melting has a higher K/Na ratio, and water-fluxed melting is just the opposite (Douce and McCarthy, 1998). The K/Na ratios of Yaozhuang stock also (0.86–1.19, avg. 1.05) support the above conclusions.

Interestingly, the water of post-collision ore-forming magma may come from additional water supplementation (Wang et al., 2018). One theory is that the water-rich mantle-derived ultra-potassium magma is mixed with the lower crustal magma to provide water (Yang et al., 2015), and the other explains that the subduction of continental crust dehydration releases free fluids into the magma to increase the water content of the magma (Zheng, 2009,; Zheng, 2019).

Researchers previously proposed that 10,000*(Eu/Eu*)/Y and Eu/Eu* ratios are positively correlated with Ce/Nd ratios, which can well indicate the oxygen fugacity of wet fertile magmatic–hydrothermal solution. The best fertility indicators are zircon Eu/Eu* (>0.3), 10,000·(Eu/Eu*)/Y (>1) ratios, and (Ce/Nd)/Y (>0.01) (Lu et al., 2016; Zheng et al., 2021). The above zircon trace element ratios of the Yaozhuang stock plot in the high-oxygen fugacity fertile magma region (**Figures 11C,D**). In addition, the zircon Delta FMQ values of porphyritic granite (avg. +2.7, the calculation method is derived from Li et al., 2019) and monzogranite (avg. + 3.9) in this study are higher than the basic conditions of porphyry mineralization (Delta FMQ > 1.5).

Porphyry-type mineralization is commonly associated with porphyry stocks, where large amounts of ore-forming fluids and materials were focused into the intrusion apex to form disseminated or vein-type ores (Hedenquist and Lowenstern, 1994; Heinrich, 2005; Blundy et al., 2015). Field geological surveys show that the mineralization and alterations are generally developed, such as Mo mineralization and silicic, pyrite, and sericite alterations. The molybdenite filled the wall rock fractures (**Figure 2A**), which indicates that the Yaozhuang area has the potential to prospect porphyry Mo deposits.

## CONCLUSION

(1) The newly discovered porphyritic granite and monzogranite in the Yaozhuang area are zircon U-Pb dated to be 157 ± 2 and 153 ± 1 Ma, coeval with the magmatic peak of the region.
(2) The high-K calc-alkaline Yaozhuang I-type granites are metaluminous–weakly peraluminous, with zircon $\varepsilon_{Hf}(t)$ values of −16.1 to −6.9 and $t_{DM2}$ ages of 1.78–2.16 Ga. The granites may have formed from partial melting of the lower crust mixed with some mantle components.
(3) The Yaozhuang granitic stocks were likely formed by the lower crustal delamination in North Qinling. The asthenospheric upwelling may have heated the lithospheric mantle to form mantle-derived magma, which then caused the lower crustal melting and magma mixing. These magmas were finally emplaced into the fault intersections at Yaozhuang.

## DATA AVAILABILITY STATEMENT

The original contributions presented in the study are included in the article/Supplementary Material, further inquiries can be directed to the corresponding author.

## AUTHOR CONTRIBUTIONS

PF: conceived the research, investigated the literature, and wrote the manuscript. AX, BZ, and XC: provided research funds, supervision, and revision. WY, JS, HZ, and LW: participated in data analysis and academic support. All authors contributed to the article and approved the submitted version.

## FUNDING

This study was financially supported by the National Natural Science Foundation of China (No. 41272095), the Geological Exploration Funds of Shaanxi Province (No. 61201908334), and Public Welfare Geological Survey Funds of Shaanxi Province (202112).

## ACKNOWLEDGMENTS

We would like to express our sincere thanks to Associate Editor KL and the two reviewers for their valuable comments and suggestions and to Prof. Yunpeng Dong of Northwestern University for his kind assistance on the manuscript.

## REFERENCES

Andersen, T. (2002). Correction of Common lead in U-Pb Analyses that Do Not Report 204Pb. *Chem. Geology.* 192, 59–79. doi:10.1016/S0009-2541(02)00195-X

Bao, Z. W., Wang, C. Y., Zeng, L. J., Sun, W. D., and Yao, J. M. (2015). Slab Break-Off Model for the Triassic Syn-Collisional Granites in the Qinling Orogenic belt, Central China: Zircon U-Pb Age and Hf Isotope Constraints. *Int. Geology. Rev.* 57, 492–507. doi:10.1080/00206814.2015.1017777

Bao, Z. W., Xiong, M. F., and Li, Q. (2019). Petrogenesis of Late Mesozoic High-Ba-Sr Granites in the Qiushuwan Cu Mo orefield: Implications for the Distribution of Porphyry Mo Mineralization in the East Qinling Area of Central China. *Lithos* 348-349, 105172–111072. doi:10.1016/j.lithos.2019.105172

Belousova, E., Griffin, W., O'Reilly, S. Y., and Fisher, N. (2002). Igneous Zircon: Trace Element Composition as an Indicator of Source Rock Type. *Contrib. Mineral. Petrol.* 143, 602–622. doi:10.1007/s00410-002-0364-7

Blundy, J., Mavrogenes, J., Tattitch, B., Sparks, S., and Gilmer, A. (2015). Generation of Porphyry Copper Deposits by Gas-Brine Reaction in Volcanic Arcs. *Nat. Geosci* 8, 235–240. doi:10.1038/ngeo2351

Blundy, J., and Wood, B. (1994). Prediction of crystal-melt Partition Coefficients from Elastic Moduli. *Nature* 372, 452–454. doi:10.1038/372452a0

Burnham, A. D., and Berry, A. J. (2012). An Experimental Study of Trace Element Partitioning between Zircon and Melt as a Function of Oxygen Fugacity. *Geochimica et Cosmochimica Acta* 95, 196–212. doi:10.1016/j.gca.2012.07.034

Chen, L., Yan, Z., Guo, X., and Fu, C. (2019). Melting of the Meso-Neoproterozoic Juvenile Crust for the Origin of the Late Triassic Mo Mineralization in South Qinling, central China: Evidence from Geochronology and Geochemistry of the Yangmugou deposit. *J. Asian Earth Sci.* 174, 109–125. doi:10.1016/j.jseaes.2018.11.022

Davidson, J., Turner, S., Handley, H., Macpherson, C., and Dosseto, A. (2007). Amphibole "Sponge" in Arc Crust. *Geol* 35, 787–790. doi:10.1130/G23637A.1

Ding, L. X., Ma, C. Q., Li, J. W., Robinson, P. T., Deng, X. D., Zhang, C., et al. (2011). Timing and Genesis of the Adakitic and Shoshonitic Intrusions in the Laoniushan Complex, Southern Margin of the North China Craton: Implications for post-collisional Magmatism Associated with the Qinling Orogen. *Lithos* 126, 212–232. doi:10.1016/j.lithos.2011.07.008

Diwu, C. R., Sun, Y., Liu, L., Zhang, C. L., and Wang, H. L. (2010). The Disintegration of Kuanping Group in North Qinling Orogenic Belts and Neo-Proterozoic N-MORB. Acta Petrol. *Sin* 26, 2025–2038.

Diwu, C. R., Sun, Y., Zhao, Y., Liu, B. X., and Lai, S. C. (2014). Geochronological, Geochemical, and Nd-Hf Isotopic Studies of the Qinling Complex, central China: Implications for the Evolutionary History of the North Qinling Orogenic Belt. *Geosci. Front.* 5, 499–513. doi:10.1016/10.1016/j.gsf.2014.04.001

Dong, G. C., Santosh, M., Li, S. R., Shen, J. F., Mo, X. X., Scott, S., et al. (2013). Mesozoic Magmatism and Metallogenesis Associated with the Destruction of the North China Craton: Evidence from U-Pb Geochronology and Stable Isotope Geochemistry of the Mujicun Porphyry Cu-Mo deposit. *Ore Geology. Rev.* 53, 434–445. doi:10.1016/j.oregeorev.2013.02.006

Dong, S. W., Zhang, Y. Q., Li, H. L., Shi, W., Xue, H. M., Li, J. H., et al. (2018). The Yanshan Orogeny and Late Mesozoic Multi-Plate Convergence in East Asia-Commemorating 90th Years of the "Yanshan Orogeny". *Sci. China Earth Sci.* 61, 1888–1909. doi:10.1007/s11430-017-9297-y

Dong, Y., Liu, X., Zhang, G., Chen, Q., Zhang, X., Li, W., et al. (2012). Triassic Diorites and Granitoids in the Foping Area: Constraints on the Conversion from Subduction to Collision in the Qinling Orogen, China. *J. Asian Earth Sci.* 47, 123–142. doi:10.1016/j.jseaes.2011.06.005

Dong, Y., Zhang, G., Neubauer, F., Liu, X., Genser, J., and Hauzenberger, C. (2011a). Tectonic Evolution of the Qinling Orogen, China: Review and Synthesis. *J. Asian Earth Sci.* 41, 213–237. doi:10.1016/j.jseaes.2011.03.002

Douce, A. E. P., and McCarthy, T. C. (1998). "Melting of Crustal Rocks during Continental Collision and Subduction," in *When Continents Collide: Geodynamics and Geochemistry of Ultrahigh-Pressure Rocks*. Editors B. R. Hacker and J. G. Liou (Dordrecht: Springer), 27–55. doi:10.1007/978-94-015-9050-1_2*Melting of Crustal Rocks during continental Collision and Subduction*

Fan, H. R., and Xie, Y. H. (1999). Porphyry Type Molybdenum Deposits in the Eastern Qinling Mo belt. *Cent. China. Sci. Geol. Sin* 8, 91–101.

Gao, X., and Zhao, T. (2017). Late Mesozoic Magmatism and Tectonic Evolution in the Southern Margin of the North China Craton. *Sci. China Earth Sci.* 60, 1959–1975. doi:10.1007/s11430-016-9069-0

Harris, N. B. W., Tindle, A. J. A., and Tindle, G. (1986). Geochemical Characteristics of Collision-Zone Magmatism. *Geol. Soc. Lond. Spec. Publications* 19, 67–81. doi:10.1144/gsl.sp.1986.019.01.04

He, Y., Li, S., Hoefs, J., Huang, F., Liu, S.-A., and Hou, Z. (2011). Post-collisional Granitoids from the Dabie Orogen: New Evidence for Partial Melting of a Thickened continental Crust. *Geochimica et Cosmochimica Acta* 75, 3815–3838. doi:10.1016/j.gca.2011.04.011

Hedenquist, J. W., and Lowenstern, J. B. (1994). The Role of Magmas in the Formation of Hydrothermal Ore Deposits. *Nature* 370, 519–527. doi:10.1038/370519a0

Heinrich, C. A. (2005). The Physical and Chemical Evolution of Low-Salinity Magmatic Fluids at the Porphyry to Epithermal Transition: A Thermodynamic Study. *Miner Deposita* 39, 864–889. doi:10.1007/s00126-004-0461-9

Hu, H., Li, J.-W., McFarlane, C. R. M., Luo, Y., and McCarron, T. (2017). Textures, Trace Element Compositions, and U-Pb Ages of Titanite from the Mangling Granitoid Pluton, East Qinling Orogen: Implications for Magma Mixing and Destruction of the North China Craton. *Lithos* 284-285, 50–68. doi:10.1016/j.lithos.2017.03.025

Inger, S., and Harris, N. (1993). Geochemical Constraints on Leucogranite Magmatism in the Langtang Valley, Nepal Himalaya. *J. Petrol.* 34, 345–368. doi:10.1093/petrology/34.2.345

Jingwen, M., Yanbo, C., Maohong, C., and Pirajno, F. (2013). Major Types and Time-Space Distribution of Mesozoic Ore Deposits in South China and Their Geodynamic Settings. *Miner Deposita* 48, 267–294. doi:10.1007/s00126-012-0446-z

Joseph, B. W., Kenneth, L. C., and Bruce, W. C. (1987). A-type Granites: Geochemical Characteristics, Discrimination and Petrogenesis. *Contrib. Mineral. Petrol.* 95, 407–419.

Ke, C. H., Wang, X. X., Li, J. B., and Qi, Q. J. (2012a). Geochronology and Geological Significance of the Granites from the Mahe Mo deposit in the North Qinling. Acta Petrol. *Sin* 28, 267–278.

Ke, C. H., Wang, X. X., Yang, Y., Qi, Q. J., Fan, Z. P., Gao, F., et al. (2012b). *Rock-forming and Ore-Forming Ages of the Nantai Mo Polymetallic deposit in North Qinling Mountains and its Zircon Hf Isotope Composition: Geology. China* 39, 1562–1576

Kelemen, P. B. (1995). Genesis of High Mg# Andesites and the continental Crust. *Contr. Mineral. Petrol.* 120, 1–19. doi:10.1007/BF00311004

Kemp, A. I. S., Hawkesworth, C. J., Foster, G. L., Paterson, B. A., Woodhead, J. D., Hergt, J. M., et al. (2007). Magmatic and Crustal Differentiation History of Granitic Rocks from Hf-O Isotopes in Zircon. *Science* 315, 980–983. doi:10.1126/science.1136154

Kinny, P. D., and Maas, R. (2003). 12. Lu-Hf and Sm-Nd Isotope Systems in Zircon. *Rev. Mineral. Geochem.* 53, 327–342. doi:10.1515/9781501509322-015

Kröner, A., Compston, W., Guo-wei, Z., An-lin, G., and Todt, W. (1988). Age and Tectonic Setting of Late Archean Greenstone-Gneiss Terrain in Henan Province, China, as Revealed by Single-Grain Zircon Dating. *Geol* 16, 211. doi:10.1130/0091-7613(1988)01610.1130/0091-7613(1988)016<0211:aatsol>2.3.co;2

Lei, W., Dai, J., Zhao, T., Zhang, Y., and Tao, N. (2018). Field Geology, Geochronology, and Isotope Geochemistry of the Luyuangou Gold deposit, China: Implications for the Gold Mineralization in the Eastern Qinling Orogen. *Geol. J.* 53, 96–112. doi:10.1002/gj.3064

Li, N., Chen, Y. J., Santosh, M., and Pirajno, F. (2015). Compositional Polarity of Triassic Granitoids in the Qinling Orogen, China: Implication for Termination of the Northernmost Paleo-Tethys. *Gondwana Res.* 27, 244–257. doi:10.1016/j.gr.2013.09.017

Li, W., Cheng, Y., and Yang, Z. (2019). Geo- F O 2 : Integrated Software for Analysis of Magmatic Oxygen Fugacity. *Geochem. Geophys. Geosyst.* 20, 2542–2555. doi:10.1029/2019GC008273

Li, Z. X., and Li, X. H. (2007). Formation of the 1300-km-wide Intracontinental Orogen and Postorogenic Magmatic Province in Mesozoic South China: A Flat-Slab Subduction Model. *Geol* 35, 179. doi:10.1130/G23193A.1

Li, C. D., Zhao, L. G., Xu, Y. W., Chang, Q. S., Wang, S. Y., and Xu, T. (2018). Chronology of Metasedimentary Rocks from Kuanping Group Complex in North Qinling Belt and its Geological Significance. *Geology. China* 45, 992–1010

Li, N., Chen, Y. J., Santosh, M., and Pirajno, F. (2018). Late Mesozoic Granitoids in the Qinling Orogen, Central China, and Tectonic Significance. *Earth-Science Rev.* 182, 141–173. doi:10.1016/j.earscirev.2018.05.004

Liang, T., Li, L.-M., Lu, R., and Xiao, W.-J. (2020). Early Cretaceous Mafic Dikes in the Northern Qinling Orogenic Belt, central China: Implications for Lithosphere Delamination. *J. Asian Earth Sci.* 194, 104142. doi:10.1016/j.jseaes.2019.104142

Liu, B. X., Qi, Y., Wang, W., Siebel, W., Zhu, X. Y., Nie, H., et al. . (2013). Zircon U-Pb Ages and O-Nd Isotopic Composition of Basement Rocks in the North Qinling Terrain, central China: Evidence for Provenance and Evolution. *Int. J. Earth Sci. (Geol Rundsch)* 102, 2153–2173. doi:10.1007/s00531-013-0912-6

Liu, L., Liao, X., Wang, Y., Wang, C., Santosh, M., Yang, M., et al. (2016). Early Paleozoic Tectonic Evolution of the North Qinling Orogenic Belt in Central China: Insights on continental Deep Subduction and Multiphase Exhumation. *Earth-Science Rev.* 159, 58–81. doi:10.1016/j.earscirev.2016.05.005

Liu, R., Chen, M., Tian, X. S., Hu, Y., and Yang, D. P. (2014). Geochemical, Zircon SIMS U-Pb Geochronological and Hf Isotopic Study on Nantian and Muhuguan Plutons in Eastern Qinling, China: Petrogenesis and Tectonic Implications. Acta Miner. *Sin* 34, 469–480

Liu, Y., Hu, Z., Zong, K., Gao, C., Gao, S., Xu, J., et al. (2010). Reappraisement and Refinement of Zircon U-Pb Isotope and Trace Element Analyses by LA-ICP-MS. *Chin. Sci. Bull.* 55, 1535–1546. doi:10.1007/s11434-010-3052-4

Liu, R., Li, J. W., Bi, S. J., Hu, H., and Chen, M. (2013). Magma Mixing Revealed from *In Situ* Zircon U-Pb-Hf Isotope Analysis of the Muhuguan Granitoid Pluton, Eastern Qinling Orogen, China: Implications for Late Mesozoic Tectonic Evolution. *Int. J. Earth Sci. (Geol Rundsch)* 102, 1583–1602. doi:10.1007/s00531-013-0900-x

Lu, Y. F. (2004). GeoKit: A Geochemical Toolkit for Microsoft Excel. *Geochimica* 33, 459–464

Lu, Y. J., Loucks, R. R., Fiorentini, M., McCuaig, T. C., Evans, N. J., Yang, Z. M., et al. (2016). *Zircon Compositions as a Pathfinder for Porphyry Cu ± Mo ± Au Deposits. Tectonics Metallog Tethyan Orog.* doi:10.5382/SP.19.13

Maniar, P. D., and Piccoli, P. M. (1989). Tectonic Discrimination of Granitoids. *Geol. Soc. Am. Bull.* 101, 635–643. doi:10.1130/0016-7606(1989)101<0635:TDOG>2.3.CO;2

Mao, J. W., Xie, G. Q., Pirajno, F., Ye, H. S., Wang, Y. B., Li, Y. F., et al. (2010). Late Jurassic-Early Cretaceous Granitoid Magmatism in Eastern Qinling, central-eastern China: SHRIMP Zircon U-Pb Ages and Tectonic Implications. *Aust. J. Earth Sci.* 57, 51–78. doi:10.1080/08120090903416203

Mao, J. W., Pirajno, F., Xiang, J. F., Gao, J. J., Ye, H. S., Li, Y. F., et al. (2011). Mesozoic Molybdenum Deposits in the East Qinling-Dabie Orogenic belt: Characteristics and Tectonic Settings. *Ore Geology. Rev.* 43, 264–293. doi:10.1016/j.oregeorev.2011.07.009

Mao, J. W., Xie, G. Q., Bierlein, F., Qü, W. J., Du, A. D., Ye, H. S., et al. (2008). Tectonic Implications from Re-os Dating of Mesozoic Molybdenum Deposits in the East Qinling-Dabie Orogenic belt. *Geochimica et Cosmochimica Acta* 72, 4607–4626. doi:10.1016/j.gca.2008.06.027

Mao, J., Xiong, B., Liu, J., Pirajno, F., Cheng, Y., Ye, H., et al. (2017). Molybdenite Re/Os Dating, Zircon U-Pb Age and Geochemistry of Granitoids in the Yangchuling Porphyry W-Mo deposit (Jiangnan Tungsten Ore belt), China: Implications for Petrogenesis, Mineralization and Geodynamic Setting. *Lithos* 286-287, 35–52. doi:10.1016/j.lithos.2017.05.023

Mattauer, M., Matte, P., Malavieille, J., Tapponnier, P., Maluski, H., Qin, X. Z., et al. (1985). Tectonics of the Qinling Belt: Build-Up and Evolution of Eastern Asia. *Nature* 317, 496–500. doi:10.1038/317496a0

Meng, F., Mao, J. W., Ye, H. S., Zhou, K., Gao, Y. L., Li, Y. F., et al. (2012). Zircon SHRIMP U-Pb Dating and Geochemistry of the Laojunshan Intrusion,Western Henan Province. *Geology. China* 39, 1501–1524.

Meng, J., Xia, X., Ma, L., Jiang, Z., Xu, J., Cui, Z., et al. (2021). A H2O-In-Zircon Perspective on the Heterogeneous Water Content of Crust-Derived Magmas in Southern Tibet. *Sci. China Earth Sci.* 64, 1184–1194. doi:10.1007/s11430-020-9790-1

Meng, Q. R., and Zhang, G. W. (1999). Timing of Collision of the North and South China Blocks: Controversy and Reconciliation. *Geology* 27, 1–96. doi:10.1130/0091-7613(1999)0272.3.CO;2

Naney, M. T. (1983). Phase Equilibria of Rock-Forming Ferromagnesian Silicates in Granitic Systems. *Am. J. Sci.* 283, 993–1033. doi:10.2475/ajs.283.10.993

Park, J. W., Campbell, I. H., Chiaradia, M., Hao, H., and Lee, C. T. (2021). Crustal Magmatic Controls on the Formation of Porphyry Copper Deposits. *Nat. Rev. Earth Environ.* 2, 542–557. doi:10.1038/s43017-021-00182-8

Pearce, J. (1996). Sources and Settings of Granitic Rocks. *Episodes* 19, 120–125. doi:10.18814/epiiugs/1996/v19i4/005

Peccerillo, A., and Taylor, S. R. (1976). Geochemistry of Eocene Calc-Alkaline Volcanic Rocks from the Kastamonu Area, Northern Turkey. *Contr. Mineral. Petrol.* 58, 63–81. doi:10.1007/BF00384745

Qin, H. P., Wu, C. L., Wu, X. P., Lei, M., and Hou, Z. H. (2012). LA-ICP-MS Zircon U-Pb Ages and Implications for Tectonic Setting of the Mangling Granitoid Plutons in Qinling Orogen belt. *Geol. Rev.* 58, 783–792.

Rapp, R. P., Shimizu, N., Norman, M. D., and Applegate, G. S. (1999). Reaction between Slab-Derived Melts and Peridotite in the Mantle Wedge: Experimental Constraints at 3.8 GPa. *Chem. Geology.* 160, 335–356. doi:10.1016/S0009-2541(99)00106-0

Ratschbacher, L., Hacker, B. R., Calvert, A., Webb, L. E., Grimmer, J. C., McWilliams, M. O., et al. (2003). Tectonics of the Qinling (Central China): Tectonostratigraphy, Geochronology, and Deformation History. *Tectonophysics* 366, 1–53. doi:10.1016/S0040-1951(03)00053-2

Richards, J. P. (2011). Magmatic to Hydrothermal Metal Fluxes in Convergent and Collided Margins. *Ore Geology. Rev.* 40, 1–26. doi:10.1016/j.oregeorev.2011.05.006

Richards, J. P., Spell, T., Rameh, E., Razique, A., and Fletcher, T. (2012). High Sr/Y Magmas Reflect Arc Maturity, High Magmatic Water Content, and Porphyry Cu ± Mo ± Au Potential: Examples from the Tethyan Arcs of Central and Eastern Iran and Western Pakistan. *Econ. Geol.* 107, 295–332. doi:10.2113/econgeo.107.2.295

Ridolfi, F., Renzulli, A., and Puerini, M. (2010). Stability and Chemical Equilibrium of Amphibole in Calc-Alkaline Magmas: An Overview, New Thermobarometric Formulations and Application to Subduction-Related Volcanoes. *Contrib. Mineral. Petrol.* 160, 45–66. doi:10.1007/s00410-009-0465-7

Rudnick, R. L., and Gao, S. (2003). Composition of the continental Crust. *Treatise Geochem.* 3, 1–64. doi:10.1016/b0-08-043751-6/03016-4

Sillitoe, R. H. (2010). Porphyry Copper Systems. *Econ. Geology.* 105, 3–41. doi:10.2113/gsecongeo.105.1.3

Smithies, R. H., and Champion, D. C. (2000). The Archaean High-Mg Diorite Suite: Links to Tonalite-Trondhjemite-Granodiorite Magmatism and Implications for Early Archaean Crustal Growth. *J. Petrol.* 41, 1653–1671. doi:10.1093/petrology/41.12.1653

Sun, S. S., and McDonough, W. F. (1989). Chemical and Isotopic Systematics of Oceanic Basalts: Implications for Mantle Composition and Processes. *Geol. Soc. Lond. Spec. Publications* 42, 313–345. doi:10.1144/GSL.SP.1989.042.01.19

Sylvester, P. J. (1998). Post-collisional Strongly Peraluminous Granites. *Lithos* 45, 29–44. doi:10.1016/S0024-4937(98)00024-3

Vervoort, J. D., Patchett, P. J., Gehrels, G. E., and Nutman, A. P. (1996). Constraints on Early Earth Differentiation from Hafnium and Neodymium Isotopes. *Nature* 379, 624–627. doi:10.1038/379624a0

Wang, C., Deng, J., Bagas, L., and Wang, Q. (2017). Zircon Hf-Isotopic Mapping for Understanding Crustal Architecture and Metallogenesis in the Eastern Qinling Orogen. *Gondwana Res.* 50, 293–310. doi:10.1016/j.gr.2017.04.008

Wang, R., Luo, C. H., Xia, W. J., Sun, Y. C., Liu, B., and Zhang, J. B. (2021). Progresses in the Study of High Magmatic Water and Oxidation State of Post-Collisional Magmas in the Gangdese Porphyry Deposit Belt. Bull Miner. Petrol. *Geochem* 40, 1061–1077

Wang, R., Richards, J. P., Hou, Z. Q., Yang, Z. Q., Gou, Z. B., and DuFrane, S. A. (2014b). Increasing Magmatic Oxidation State from Paleocene to Miocene in the Eastern Gangdese Belt, Tibet: Implication for Collision-Related Porphyry Cu-Mo Au Mineralization. *Econ. Geology.* 109, 1943–1965. doi:10.2113/econgeo.109.7.1943

Wang, R., Richards, J. P., Hou, Z., Yang, Z., and DuFrane, S. A. (2014a). Increased Magmatic Water Content--The Key to Oligo-Miocene Porphyry Cu-Mo Au Formation in the Eastern Gangdese Belt, Tibet. *Econ. Geology.* 109, 1315–1339. doi:10.2113/econgeo.109.5.1315

Wang, R., Weinberg, R. F., Collins, W. J., Richards, J. P., and Zhu, D.-c. (2018). Origin of Postcollisional Magmas and Formation of Porphyry Cu Deposits in Southern Tibet. *Earth-Science Rev.* 181, 122–143. doi:10.1016/j.earscirev.2018.02.019

Wang, T., Guo, L., Zheng, Y. D., Donskaya, T., Dmirty, G., Zeng, L. S., et al. (2012). Timing and Processes of Late Mesozoic Mid-lower-crustal Extension in continental NE Asia and Implications for the Tectonic Setting of the Destruction of the North China Craton: Mainly Constrained by Zircon U-Pb Ages from Metamorphic Core Complexes. *Lithos* 154, 315–345. doi:10.1016/j.lithos.2012.07.020

Wang, T. H., Mao, J. W., and Wang, Y. B. (2008). Research on SHRIMP Chronology in Xiaoqinling-Xionger'Shan Area: The Evidence of Delamination of Lithosphere in Qinling Orogenic belt. Acta Petrol. *Sin* 24, 1273–1287.

Wang, X. X., Wang, T., Ke, C., Yang, Y., Li, J., Li, Y., et al. (2015a). Nd-Hf Isotopic Mapping of Late Mesozoic Granitoids in the East Qinling Orogen, central China: Constraint on the Basements of Terranes and Distribution of Mo Mineralization. *J. Asian Earth Sci.* 103, 169–183. doi:10.1016/j.jseaes.2014.07.002

Wang, X. X., Wang, T., and Zhang, C. (2015b). Granitoid Magmatism in the Qinling Orogen, Central China and its Bearing on Orogenic Evolution. *Sci. China Earth Sci.* 58, 1497–1512. doi:10.1007/s11430-015-5150-2

Wang, X. X., Wang, T., and Zhang, C. (2013). Neoproterozoic, Paleozoic, and Mesozoic Granitoid Magmatism in the Qinling Orogen, China: Constraints on Orogenic Process. *J. Asian Earth Sci.* 72, 129–151. doi:10.1016/j.jseaes.2012.11.037

Wang, X. X., Wang, T., Qi, Q. J., and Li, S. (2011). Temporal Spatial Variations, Origin and Their Tectonic Significance of the Late Mesozoic Granites in the Qinling, Central China. Acta Petrol. *Sin* 27, 1573–1593.

Wang, Y., Zhang, Y. S., Cheng, H., and Chen, F. (2020). Complex Magma Sources of Late Mesozoic Granites along the Southern Margin of the North China Craton: Constraints from Geochemistry and Geochronology of the Massive Heyu and Lantian Plutons. *Int. Geology. Rev.* 62, 1862–1882. doi:10.1080/00206814.2019.1669078

Weinberg, R. F., and Hasalová, P. (2015). Water-fluxed Melting of the continental Crust: A Review. *Lithos* 212-215, 158–188. doi:10.1016/j.lithos.2014.08.021

Wilson, M. (1989). Igneous Petrogenesis: A Global Tectonic Approach: Boston, MA, Unwin Hyman. *ISBN* 0045520259, 496.

Wu, F. Y., Liu, X. C., Ji, W. Q., Wang, J. M., and Yang, L. (2017). Highly Fractionated Granites: Recognition and Research. *Sci. China Earth Sci.* 60, 1201–1219. doi:10.1007/s11430-016-5139-1

Wu, F. Y., Li, X. H., Yang, J. H., and Zheng, Y. F. (2007b). Discussions on the Petrogenesis of Granites. Acta Petrol. *Sin* 23, 1217–1238.

Wu, F. Y., Li, X. H., Zheng, Y. F., and Gao, S. (2007a). Lu-Hf Isotopic Systematics and Their Applications in Petrology. Acta Petrol. *Sin* 23, 185–220.

Wu, Y. B., and Zheng, Y. F. (2004). Genesis of Zircon and its Constraints on Interpretation of U-Pb Age. *Chin.Sci.Bull.* 49, 1554–1569. doi:10.1007/BF03184122

Xu, P., Wu, F., Xie, L., and Yang, Y. (2004). Hf Isotopic Compositions of the Standard Zircons for U-Pb Dating. *Chin.Sci.Bull.* 49, 1642–1648. doi:10.1360/04wd012810.1007/bf03184136

Xu, Y. G., Ma, J. L., Huang, X. L., Iizuka, Y., Chung, S. L., Wang, Y. B., et al. (2004). Early Cretaceous Gabbroic Complex from Yinan, Shandong Province: Petrogenesis and Mantle Domains beneath the North China Craton. *Int. J. Earth Sci. (Geol Rundsch)* 93, 1025–1041. doi:10.1007/s00531-004-0430-7

Xu, Y. G., Wang, R. C., Wang, C. Y., Linnen, R., and Wu, F. Y. (2021). Highly Fractionated Granites and Rare-Metal Mineralization. *Lithos* 398-399, 106262. doi:10.1016/j.lithos.2021.106262

Xu, Y. G., Li, H. Y., Pang, C. J., and He, B. (2009). On the Timing and Duration of the Destruction of the North China Craton. *Sci. Bull.* 54, 3379–3396. doi:10.1007/s11434-009-0346-5

Yang, H. T., Li, L., Niu, L., He, L., and Bai, X. H. (2019). Report on Survey of Molybdenum Polymetallic Deposits in the Western of Mangling Orefield in Shangzhou District-Luonan County, Xi'an, China. Northwest Nonferrous Geological Research Institute Co., Ltd.

Yang, J. H., Xu, L., Sun, J. F., Zeng, Q., Zhao, Y. N., Wang, H., et al. (2021). Geodynamics of Decratonization and Related Magmatism and Mineralization in the North China Craton. *Sci. China Earth Sci.* 64, 1409–1427. doi:10.1007/s11430-020-9732-6

Yang, Y., Liu, Z. J., and Deng, X. H. (2017). Mineralization Mechanisms in the Shangfanggou Giant Porphyry-Skarn Mo-Fe deposit of the East Qinling, China: Constraints from H-O-C-S-Pb Isotopes. *Ore Geology. Rev.* 81, 535–547. doi:10.1016/j.oregeorev.2016.06.026

Yang, Y., Wang, X. X., Ke, C. H., Li, J. B., Lv, X. Q., Meng, X. Y., et al. (2014). Zircon U-Pb Ages, Geochemistry and Evolution of Mangling Pluton in North Qinling Mountains. *Miner Deposits* 33, 14–36.

Yang, Y., Zhang, L., Xue, S. L., and Wang, S. S. (2020). Report on 1:50,000 Gravity Survey Results in Western Mangling Ore Concentration Area, Xi'an, China. Shaanxi Mineral Geological Survey Center.

Yang, Z. M., Lu, Y. J., Hou, Z. Q., and Chang, Z. S. (2015). High-Mg Diorite from Qulong in Southern Tibet: Implications for the Genesis of Adakite-like Intrusions and Associated Porphyry Cu Deposits in Collisional Orogens. *J. Petrol.* 56, 227–254. doi:10.1093/petrology/egu076

Yuan, H. L., Gao, S., Dai, M. N., Zong, C. L., Günther, D., Fontaine, G. H., et al. (2008). Simultaneous Determinations of U-Pb Age, Hf Isotopes and Trace Element Compositions of Zircon by Excimer Laser-Ablation Quadrupole and Multiple-Collector ICP-MS. *Chem. Geology.* 247, 100–118. doi:10.1016/j.chemgeo.2007.10.003

Yuan, H. L., Wu, F. Y., Gao, S., Liu, X. M., Xu, P., and Sun, D. Y. (2003). Determination of U-Pb Age and Rare Earth Element Concentrations of Zircons from Cenozoic Intrusions in Northeastern China by Laser Ablation ICP-MS. *Chin. Sci. Bull.* 48, 1511–1520.

Zeng, Q. D., Liu, J. M., Chu, S. X., Wang, Y. B., Sun, Y., Duan, X. X., et al. (2012). Mesozoic Molybdenum Deposits in the East Xingmeng Orogenic belt, Northeast China: Characteristics and Tectonic Setting. *Int. Geology. Rev.* 54, 1843–1869. doi:10.1080/00206814.2012.677498

Zhai, M. G., and Santosh, M. (2013). Metallogeny of the North China Craton: Link with Secular Changes in the Evolving Earth. *Gondwana Res.* 24, 275–297. doi:10.1016/j.gr.2013.02.007

Zhang, G. W., Zhang, Z. Q., and Dong, Y. P. (1995). Nature of Main Tectono-Lithostratigraphic Units of the Qinling Orogen: Implications for the Tectonic Evolution. Acta Petrol. *Sin* 11, 101–114.

Zhang, H. F., Yu, H., Zhou, D. W., Zhang, J., Dong, Y. P., and Zhang, G. W. (2015). The Meta-Gabbroic Complex of Fushui in north Qinling Orogen: A Case of Syn-Subduction Mafic Magmatism. *Gondwana Res.* 28, 262–275. doi:10.1016/j.gr.2014.04.010

Zhang, H., Li, S. Q., Fang, B. W., He, J. F., Xue, Y. Y., Siebel, W., et al. (2018). Zircon U-Pb Ages and Geochemistry of Migmatites and Granites in the Foping Dome: Evidence for Late Triassic Crustal Evolution in South Qinling, China. *Lithos* 296-299, 129–141. doi:10.1016/j.lithos.2017.10.024

Zhang, S. H., Han, F. L., Wang, G. B., Wang, B. Y., and Cui, J. T. (2019). *Regional Geology of China Shaanxi Chronicles*. Beijing: Geological Publishing House, 142–186.

Zhang, Y. S., Wolfgang, S., He, S., Wang, Y., and Chen, F. K. (2019). Origin and Genesis of Late Jurassic to Early Cretaceous Granites of the North Qinling Terrane, China. *Lithos* 336-337, 242–257. doi:10.1016/j.lithos.2019.04.008

Zheng, S., An, Y., Lai, C., Wang, H., and Li, Y. (2021). Genesis of High-Mg Adakites in the Southeastern Margin of North China Craton: Geochemical and U-Pb Geochronological Perspectives. *Front. Earth Sci.* 9, 731233. doi:10.3389/feart.2021.731233

Zheng, Y. F. (2009). Fluid Regime in continental Subduction Zones: Petrological Insights from Ultrahigh-Pressure Metamorphic Rocks. *J. Geol. Soc.* 166, 763–782. doi:10.1144/0016-76492008-016R

Zheng, Y. F. (2019). Subduction Zone Geochemistry. *Geosci. Front.* 10, 1223–1254. doi:10.1016/j.gsf.2019.02.003

Zhou, X. H. (2006). Major Transformation of Subcontinental Lithosphere beneath Eastern China in the Cenozoic-Mesozoic: Review and prospect. *Earth Sci. Front.* 13, 50–64.

Zhu, L. M., Zhang, G. W., Guo, B., Lee, B., Gong, H. J., and Wang, F. (2010). Geochemistry of the Jinduicheng Mo-Bearing Porphyry and deposit, and its Implications for the Geodynamic Setting in East Qinling, P.R. China. *Geochemistry* 70, 159–174. doi:10.1016/j.chemer.2009.12.003

Zhu, L. M., Zhang, G. W., Guo, B., and Li, B. (2009). He-Ar Isotopic System of Fluid Inclusions in Pyrite from the Molybdenum Deposits in South Margin of North China Block and its Trace to Metallogenetic and Geodynamic Background. *Chin. Sci. Bull.* 54, 2479–2492. doi:10.1007/s11434-009-0047-0

**Conflict of Interest:** The authors declare that the research was conducted in the absence of any commercial or financial relationships that could be construed as a potential conflict of interest.

**Publisher's Note:** All claims expressed in this article are solely those of the authors and do not necessarily represent those of their affiliated organizations, or those of the publisher, the editors and the reviewers. Any product that may be evaluated in this article, or claim that may be made by its manufacturer, is not guaranteed or endorsed by the publisher.

*Copyright © 2022 Fan, Xi, Zhou, Chao, Yang, Sun, Zhu and Wei. This is an open-access article distributed under the terms of the Creative Commons Attribution License (CC BY). The use, distribution or reproduction in other forums is permitted, provided the original author(s) and the copyright owner(s) are credited and that the original publication in this journal is cited, in accordance with accepted academic practice. No use, distribution or reproduction is permitted which does not comply with these terms.*